bioRxiv preprint doi: https://doi.org/10.1101/2023.03.16.532898; this version posted March 18, 2023. The copyright holder for this preprint (which was not certified by peer review) is the author/funder, who has granted bioRxiv a license to display the preprint in perpetuity. It is made available under aCC-BY-NC-ND 4.0 International license.

Context-Dependent Modification of PFKFB3 in Hematopoietic Stem Cells Promotes Anaerobic Glycolysis and Ensures Stress Hematopoiesis

Short running title: PFKFB3 supports HSC stress response

Shintaro Watanuki[1,2,†], Hiroshi Kobayashi[1,†], Yuki Sugiura[3,4,✉], Masamichi Yamamoto[5], Daiki Karigane[1,2], Kohei Shiroshita[1,2], Yuriko Sorimachi[1,6], Shuhei Koide[7], Motohiko Oshima[7], Akira Nishiyama[9], Koichi Murakami[9,10], Miho Haraguchi[1], Shinpei Tamaki[1], Takehiro Yamamoto[3], Tomohiro Yabushita[8], Yosuke Tanaka[8,11], Hiroaki Honda[12], Shinichiro Okamoto[2], Nobuhito Goda[6], Tomohiko Tamura[9,10], Ayako Nakamura-Ishizu[13], Makoto Suematsu[3,14], Atsushi Iwama[7], Toshio Suda[11,15], Keiyo Takubo[1,16,✉]

[1] Department of Stem Cell Biology, Research Institute, National Center for Global Health and Medicine, Tokyo 162-8655, Japan

[2] Division of Hematology, Department of Medicine, and [3] Department of Biochemistry, Keio University School of Medicine, Tokyo 160-8582, Japan

[4] Center for Cancer Immunotherapy and Immunobiology, Kyoto University Graduate School of Medicine, Kyoto 606-8501, Japan.

[5] Department of Research Promotion and Management, National Cerebral and Cardiovascular Center, Osaka 564-8565, Japan

[6] Department of Life Sciences and Medical BioScience, Waseda University School of Advanced Science and Engineering, Tokyo 162-8480, Japan

[7] Division of Stem Cell and Molecular Medicine, Center for Stem Cell Biology and Regenerative Medicine, and [8] Division of Cellular Therapy, The Institute of Medical Science, The University of Tokyo, Tokyo 108-8639, Japan

[9] Department of Immunology, Yokohama City University Graduate School of Medicine, Kanagawa 236-0004, Japan

[10] Advanced Medical Research Center, Yokohama City University, Kanagawa 236-0004, Japan

[11] International Research Center for Medical Sciences, Kumamoto University, Kumamoto 860-0811, Japan

[12] Field of Human Disease Models, Major in Advanced Life Sciences and Medicine, Institute of Laboratory Animals, and [13] Department of Microscopic and Developmental Anatomy, Tokyo Women's Medical University, Tokyo 162-8666, Japan

[14] Live Imaging Center, Central Institute for Experimental Animals, Kanagawa 210-0821, Japan

bioRxiv preprint doi: https://doi.org/10.1101/2023.03.16.532898; this version posted March 18, 2023. The copyright holder for this preprint (which was not certified by peer review) is the author/funder, who has granted bioRxiv a license to display the preprint in perpetuity. It is made available under aCC-BY-NC-ND 4.0 International license.

[15] Cancer Science Institute of Singapore, National University of Singapore, Singapore 117599, Singapore

[16] Japan Agency for Medical Research and Development (AMED), Core Research for Evolutional Science and Technology (CREST), Tokyo 100-0004, Japan

[†] These authors contributed equally.

✉ Corresponding Authors:

Keiyo Takubo, M.D., Ph.D.
Department of Stem Cell Biology, Research Institute
National Center for Global Health and Medicine
1-21-1 Toyama, Shinjuku-ku, Tokyo 162-8655, Japan
keiyot@gmail.com / ktakubo@ri.ncgm.go.jp

Yuki Sugiura, Ph.D.
Center for Cancer Immunotherapy and Immunobiology
Kyoto University Graduate School of Medicine
Yoshida-Konoe, Sakyo-ku, Kyoto 606-8501, Japan.
yuki.sgi@gmail.com

Number of figures: 7
Number of tables: 6
Number of references: 65

Scientific category: Hematopoiesis and Stem Cells

bioRxiv preprint doi: https://doi.org/10.1101/2023.03.16.532898; this version posted March 18, 2023. The copyright holder for this preprint (which was not certified by peer review) is the author/funder, who has granted bioRxiv a license to display the preprint in perpetuity. It is made available under aCC-BY-NC-ND 4.0 International license.

Key Points

- Combined isotope tracing, mathematical modeling, and single cell ATP analysis enable high-resolution evaluation of blood cell metabolism.
- Under stress, HSCs quickly accelerate glycolysis to meet ATP demands and maintain hematopoiesis via context-dependent PFKFB3 activation.

Abstract

Metabolic pathways are plastic and rapidly change in response to stress or perturbation. Current metabolic profiling techniques require lysis of many cells, complicating the tracking of metabolic changes over time after stress in rare cells such as hematopoietic stem cells (HSCs). Here, we aimed to identify the key metabolic enzymes that define metabolic differences between steady-state and stress conditions in HSCs and elucidate their regulatory mechanisms. Through quantitative ^{13}C metabolic flux analysis of glucose metabolism using high-sensitivity glucose tracing and mathematical modeling, we found that HSCs activate the glycolytic rate-limiting enzyme phosphofructokinase (PFK) during proliferation and oxidative phosphorylation (OXPHOS) inhibition. Real-time measurement of adenosine triphosphate (ATP) levels in single HSCs demonstrated that proliferative stress or OXPHOS inhibition led to accelerated glycolysis via increased activity of PFKFB3, the enzyme regulating an allosteric PFK activator, within seconds to meet ATP requirements. Furthermore, varying stresses differentially activated PFKFB3 via PRMT1-dependent methylation during proliferative stress and via AMPK-dependent phosphorylation during OXPHOS inhibition. Overexpression of *Pfkfb3* induced HSC proliferation and promoted differentiated cell production, whereas inhibition or loss of *Pfkfb3* suppressed them. This study reveals the flexible and multilayered regulation of HSC metabolism to sustain hematopoiesis under stress and provides techniques to better understand the physiological metabolism of rare hematopoietic cells.

KEYWORDS

hematopoietic stem cell; stem cell metabolism; PFKFB3; quantitative metabolomics; mathematical modeling; single-cell metabolic profiling; adenosine triphosphate; glycolysis; stress hematopoiesis

bioRxiv preprint doi: https://doi.org/10.1101/2023.03.16.532898; this version posted March 18, 2023. The copyright holder for this preprint (which was not certified by peer review) is the author/funder, who has granted bioRxiv a license to display the preprint in perpetuity. It is made available under aCC-BY-NC-ND 4.0 International license.

Introduction

Activities governing nutrient requirements and metabolic pathways in individual cells maintain tissue homeostasis and respond to stress through metabolite production. Adenosine triphosphate (ATP), produced via cytosolic glycolysis and mitochondrial oxidative phosphorylation (OXPHOS), is the universal energy currency of all organisms; it regulates all anabolic or catabolic cellular activities[1-3]. Precise control of intracellular ATP concentrations is critical, as ATP is the rate determiner of many ATP-dependent biochemical reactions[4-9].

Hematopoietic stem cells (HSCs) are tissue stem cells at the apex of the hematopoietic hierarchy; their function is maintained throughout life by a rigorous metabolic program and a complex interplay of gene expression, epigenetic regulation, intracellular signaling, chromatin remodeling, autophagy, and environmental factors[10-14]. Conventional analyses of the metabolic programs of hematopoietic stem and progenitor cells (HSPCs) have revealed diverse differentiation potentials and cell-cycling statuses and coordinated activities that maintain hematopoiesis[15-26]. Among the HSPC fractions, HSCs possess unique cell cycle quiescence, high self-renewal and differentiation capacity in response to stimuli, and resistance to cellular stress, including reactive oxygen species and physiological aging[10,27-30]. These properties are regulated by a balance between glycolysis and mitochondrial OXPHOS, requiring biosynthesis of ATP and various macromolecules that confer resilience to stress[31]. Among the known regulators of ATP-producing pathways, glycolytic enzymes maintain HSCs and hematopoietic progenitor cells (HPCs) by regulating cellular survival and cell cycle quiescence[32-34]. Loss of mitochondrial genes in HPSCs also induces HSC differentiation defects[35-37]. Moreover, disrupting the mitochondrial complex III subunit depletes both differentiated hematopoietic cells and quiescent HSCs[21]. Although glycolysis and the tricarboxylic acid (TCA) cycle are metabolically linked, pyruvate dehydrogenase kinase activity, which can uncouple these pathways, is required to maintain HSC function[32,38].

During HSC division, cell metabolism is reprogrammed to activate fatty acid β-oxidation and purine metabolism[39-41]. Furthermore, Liang et al. reported that activated HSCs mainly rely on glycolysis as their energy source[42]. However, the mechanisms by which each ATP-producing pathway and their connections are differentially regulated between HSCs and differentiated cells at steady state, during cell cycling, or during stress remain unknown. Recently, it has been shown that deeply quiescent HSCs do not activate cell cycle under stress[43-45]. Therefore, it remains unclear whether metabolic changes such as the individual ATP-producing pathways and their interconnections occur uniformly in all HSCs, including these deeply quiescent HSCs. Furthermore,

bioRxiv preprint doi: https://doi.org/10.1101/2023.03.16.532898; this version posted March 18, 2023. The copyright holder for this preprint (which was not certified by peer review) is the author/funder, who has granted bioRxiv a license to display the preprint in perpetuity. It is made available under aCC-BY-NC-ND 4.0 International license.

the underlying hub metabolic enzyme responsible for changes in the metabolic system of HSCs under stress has not been identified. HSCs are essential for cell therapy, including HSC transplantation, and in order to comprehensively elucidate the metabolic systems that have attracted attention as their regulatory mechanisms, recent studies have included metabolomic analyses using rare cell types such as HSCs[23,46-49], as well as isotope tracer analyses of undifferentiated hematopoietic cells purified after *in vivo* administration of isotopic glucose[50]. Although these approaches are useful for obtaining comprehensive information on intracellular metabolites, they are not suited to track real-time changes in cellular metabolism at high resolution. Therefore, new approaches are necessary to analyze metabolites quantitatively and continuously without disturbing the physiological states of single cells while integrating the recently reported metabolome analysis techniques. In this study, we aimed to identify the key metabolic enzymes that define metabolic differences between steady-state and stress conditions in HSCs and elucidate their regulatory mechanisms using a quantitative and mathematical approach. Our findings provide a platform for quantitative metabolic analysis of rare cells such as HSCs, characterize the overall metabolic reprogramming of HSCs during stress loading, and highlight the key enzyme involved in this process.

Methods

Mice

C57BL/6 mice (7–16 weeks old, Ly5.2^{+}) were purchased from Japan SLC (Shizuoka, Japan). C57BL/6 mice (Ly5.1^{+}) were purchased from CLEA Japan (Shizuoka, Japan). Knock-in mice harboring GO-ATeam2[51-53] in the ROSA26 locus were generated in the Yamamoto laboratory. The GO-ATeam2 mice (8–16 weeks old) were used to analyze HSPCs. mVenus-p27K^{-} mice (17–20 weeks old) were provided by the Kitamura Laboratory at The Institute of Medical Science, The University of Tokyo and used for cell cycle analysis[54,55]. Mice were genotyped using PCR-based assays of tail DNA or transdermal enhanced green fluorescent protein (EGFP) fluorescence. All mice were maintained in the animal facility at the National Center for Global Health and Medicine Research Institute under specific pathogen-free conditions and fed ad-libitum. Mice were euthanized by cervical dislocation. All animal experiments were approved by the Institutional Animal Care and Use Committee (IACUC) at National Center for Global Health and Medicine Research Institute. Both male and female mice were used in experiments.

bioRxiv preprint doi: https://doi.org/10.1101/2023.03.16.532898; this version posted March 18, 2023. The copyright holder for this preprint (which was not certified by peer review) is the author/funder, who has granted bioRxiv a license to display the preprint in perpetuity. It is made available under aCC-BY-NC-ND 4.0 International license.

Ion chromatography mass spectrometry (IC-MS) analysis

For metabolome analysis focused on glycolytic metabolites and nucleotides, anionic metabolites were measured using an orbitrap-type MS (Q-Exactive Focus; Thermo Fisher Scientific, Waltham, MA, USA) connected to a high-performance IC system (ICS-5000+, Thermo Fisher Scientific), enabling highly selective and sensitive metabolite quantification owing to the IC-separation and Fourier Transfer MS principle[56]. The IC instrument was equipped with an anion electrolytic suppressor (Dionex AERS 500; Thermo Fisher Scientific) to convert the potassium hydroxide gradient into pure water before the sample entered the mass spectrometer. Separation was performed using a Dionex IonPac AS11-HC-4 μm IC column (Thermo Fisher Scientific). The IC flow rate was 0.25 mL/min supplemented post-column with 0.18 mL/min makeup flow of MeOH. The potassium hydroxide gradient conditions for IC separation were as follows: 1–100 mM (0–40 min), 100 mM (40–50 min), and 1 mM (50.1–60 min), with a column temperature of 30 °C. The Q-Exactive Focus mass spectrometer was operated under ESI negative mode for all detections. Full mass scan (*m/z* 70−900) was performed at a resolution of 70,000. The automatic gain control target was set at 3×10^6 ions, and the maximum ion injection time was 100 ms. Source ionization parameters were optimized with spray voltage at 3 kV, and other parameters were as follows: transfer temperature, 320 °C; S-lens level, 50; heater temperature, 300 °C; sheath gas, 36; and aux gas, 10. Metabolite amounts were quantified from calibration curve data generated based on peak areas and respective metabolite amounts. Detailed methods for sample collection and IC-MS analysis are described in **SUPPLEMENTARY METHODS**.

Time-course analysis of ATP levels in single hematopoietic cells using GO-ATeam2 system

GO-ATeam2 is a ratiometric biosensor that monitors ATP concentration through Förster resonance energy transfer (FRET) from EGFP to the monomeric version of Kusabira Orange (mKO), regardless of the sensor expression levels[52]. Surface-marker-stained bone marrow (BM) mononuclear cells (MNCs) from GO-ATeam2 mice were dispensed into basal medium (Ba-M) containing minimal salts, vitamins, and buffers (HEPES and sodium bicarbonate), but no glucose or mitochondrial substrates (Table S1), or into medium containing mitochondrial substrates, pyruvate, lactate, fatty acids, and amino acids, but no glucose (PLFA medium). The FRET/EGFP ratio was analyzed in a real-time with a BD FACSAria IIIu Cell Sorter (BD Biosciences, Franklin Lakes, NJ, USA) under ambient pressure, and ATP levels were calculated. Detailed methods for sample collection and ATP concentration calculation are provided in **SUPPLEMENTARY METHODS**.

bioRxiv preprint doi: https://doi.org/10.1101/2023.03.16.532898; this version posted March 18, 2023. The copyright holder for this preprint (which was not certified by peer review) is the author/funder, who has granted bioRxiv a license to display the preprint in perpetuity. It is made available under aCC-BY-NC-ND 4.0 International license.

Statistical analysis

Data are presented as means ± SD, unless otherwise stated. For multiple comparisons, statistical significance was determined by Tukey's multiple comparison test using the Tukey HSD function in R ×64 4.0.3 software (R Core Team, Vienna, Austria). A paired or unpaired two-tailed Student's *t*-test and two-way ANOVA with Sidak's test were used for experiments with two groups. A p-value <0.05 was considered statistically significant.

Data sharing

All relevant data are available from the corresponding author upon reasonable request.

Results

HSC cell cycling increases anaerobic glycolytic flux

To determine how cell cycle progression alters HSC metabolism *in vivo*, we intraperitoneally and intravenously treated mice with 5-fluorouracil (5-FU) to induce HSC cell cycling (Supplemental Figure 1A). For analysis after 5-FU administration, the Lineage (Lin)$^-$ Sca-1$^+$ c-Kit$^+$ (LSK) gate was expanded to include as many HSCs as possible, for example high Sca-1-expressing cells and c-Kit-high to -dim Lin$^-$ cells, based on the previous report[57] (Supplemental Figure 1B). This expanded LSK gate was consistent with the patterns of Sca-1 and c-Kit expression observed in EPCR$^+$ Lin$^-$ CD150$^+$ CD48$^-$ cells, and the presence of EPCR, as a surface marker, identified HSCs with high stem cell activity after 5-FU administration[41]. We observed a transient decrease in the number of quiescent HSCs (Ki67$^-$) and an increase in the number of cell-cycling HSCs (Ki67$^+$) on day 6 after 5-FU treatment (Supplemental Figure 1C). Along with the loss of cell quiescence, ATP concentration in HSCs decreased transiently on day 6 (Supplemental Figure 1D). Because the route of administration of 5-FU (intraperitoneal or intravenous) made no difference in the Ki67 positivity rate of HSCs (Supplemental Figure 1E), we administered 5-FU intraperitoneally for remaining experiments. Two other methods were used to test whether cell cycle progression of HSCs after 5-FU treatment depends on the expression of EPCR. First, phosphorylation of Rb (pRb), a marker of cell cycle progression[58], was analyzed in HSCs after 5-FU treatment. Analysis of EPCR$^+$ and EPCR$^-$ HSCs showed increased pRb in HSCs from 5-FU-treated mice in both fractions compared to HSCs from phosphate-buffered saline (PBS)-treated mice, regardless of EPCR expression (Supplemental Figure 1F-G). Second, we used a G_0 marker mouse line[55]. These mice expressed a fusion protein of the p27

bioRxiv preprint doi: https://doi.org/10.1101/2023.03.16.532898; this version posted March 18, 2023. The copyright holder for this preprint (which was not certified by peer review) is the author/funder, who has granted bioRxiv a license to display the preprint in perpetuity. It is made available under aCC-BY-NC-ND 4.0 International license.

inactivation mutant p27K$^-$ and the fluorescent protein mVenus (G_0 marker), allowing prospective identification of G_0 cells. We tested whether the expression of G_0 marker in HSCs was altered after 5-FU administration to the G_0 marker mice (Supplemental Figure 1H) and found that 5-FU treatment reduced the frequency of G_0 marker-positive HSCs, regardless of the EPCR expression (Supplemental Figure 1I-J). This was not observed in the PBS group. These results indicated that 5-FU administration induced cell cycle progression of entire HSCs in mice.

HSC cell cycling is preceded by the activation of intracellular ATP-related pathways that metabolize extracellular nutrients, including glucose[39,40], which are utilized in both ATP-producing and -consuming pathways, determining cellular ATP levels. Therefore, we examined the metabolic flux of glucose by performing *in vitro* IC-MS tracer analysis with uniformly carbon-labeled (U-$^{13}C_6$) glucose to determine the pathways driving changes in ATP in 5-FU-treated HSCs (Figure 1A; Table S2). To avoid metabolite changes, samples were continuously chilled on ice during cell preparation, and the process from euthanasia to cell preparation was performed in the shortest possible time (see "**Preparation and storage of in vitro U-$^{13}C_6$-glucose tracer samples**" section under "**Supplementary Methods**" for more information). We found that changes in metabolite levels before and after sorting were present but limited (Supplemental Figure 2A). This result is consistent with the finding that the cell purification process does not significantly affect metabolite levels when sufficient care is taken in cell preparation[50]. In 5-FU-treated HSCs, the levels of glycolytic metabolites derived from U-$^{13}C_6$-glucose were double those observed in PBS-treated HSCs (Figure 1B-C; Supplemental Figure 2B). The total levels of TCA cycle intermediates derived from U-$^{13}C_6$-glucose were similar between PBS- and 5-FU-treated cells (Figure 1D; Supplemental Figure 2B). Levels of U-$^{13}C_6$-glucose-derived intermediates involved in the pentose phosphate pathway (PPP) and nucleic acid synthesis (NAS) were two-fold higher in 5-FU-treated than in PBS-treated HSCs, whereas no significant differences in the levels of metabolites were observed between both groups (Figure 1E-F; Supplemental Figure 2B). Notably, the labeling rate of metabolites during the first half of glycolysis was almost 100% in both groups, allowing us to easily track the labeled metabolites (Supplemental Figure 2C-E). This was thought to be due to the rapid replacement of unlabeled metabolites with labeled metabolites during exposure to U-$^{13}C_6$-glucose because of the generally rapid glycolytic reaction. Next, we evaluated whether glucose uptake in HSCs after 5-FU administration was differentially affected by the expression of EPCR. The fluorescent analog of glucose, 2-(N-(7-nitrobenz-2-oxa-1,3-diazol-4-yl)amino)-2-deoxyglucose (2-NBDG), was administered intravenously to mice[50] and its uptake in EPCR$^+$ and EPCR$^-$ HSCs was assayed (Figure

bioRxiv preprint doi: https://doi.org/10.1101/2023.03.16.532898; this version posted March 18, 2023. The copyright holder for this preprint (which was not certified by peer review) is the author/funder, who has granted bioRxiv a license to display the preprint in perpetuity. It is made available under aCC-BY-NC-ND 4.0 International license.

1G). Regardless of the EPCR expression, the 2-NBDG uptake was greater in HSCs treated with 5-FU than in those treated with PBS (Figure 1H-J). Furthermore, compared with HSCs cultured under quiescence-maintaining conditions, those cultured under proliferative conditions were more resistant to OXPHOS inhibition by oligomycin (Supplemental Figure 1H; Table S1). Overall, the results showed that 5-FU-treated HSCs exhibited activated glycolytic flux, increasing the turnover of ATP. Moreover, glycolytic flux into mitochondria was equally unchanged in PBS- and 5-FU-treated-HSCs, supporting that 5-FU activated anaerobic glycolysis in HSCs.

OXPHOS-inhibited HSCs exhibit compensatory glycolytic flux

Previous studies using mouse models of mitochondrial disease or defects in genes involved in electron transport chain and OXPHOS suggest that mitochondrial energy production is essential for maintaining HSC function[21,35-37], as is the glycolytic system. However, there have been no quantitative reports on how OXPHOS-inhibited HSCs can adapt their metabolism. To understand HSC metabolism under OXPHOS inhibition, we performed *in vitro* U-$^{13}C_6$-glucose tracer analysis of oligomycin-treated HSCs (Figure 2A; Table S3). Similar to 5-FU-treated HSCs (Figure 1), oligomycin-treated HSCs exhibited glycolytic system activation (Figure 2B-C; Supplemental Figure 2B). Metabolite flux to the TCA cycle and PPP was unchanged, but flux to the NAS was significantly reduced in oligomycin-treated HSCs compared to that in steady-state HSCs (Figure 2D-F; Supplemental Figure 2B). The results suggested that OXPHOS-inhibited HSCs activated compensatory glycolytic flux and suppressed NAS flux. As with 5-FU-treated HSCs, analysis of oligomycin-treated HSCs also showed almost 100% labeling of metabolites in the first half of glycolysis (Supplemental Figure 2F-H), allowing us to easily track the labeled metabolites. To further validate the compensatory glycolytic activation of HSCs under OXPHOS inhibition, a Mito Stress test was performed on HSCs and other differentiated myeloid progenitors (MyPs, Lin$^-$Sca-1$^-$c-Kit$^+$ (LKS$^-$) cells). The results showed that extracellular acidification rates (ECAR) were elevated in HSCs after oligomycin treatment compared to before oligomycin treatment (Figure 2G-H). No increase in ECAR was observed in MyPs (Figure 2G-H), supporting that inhibition of OXPHOS activated anaerobic glycolysis specifically in HSCs.

Phosphofructokinase (PFK) metabolism in HSCs is activated during proliferation and OXPHOS inhibition

To investigate whether glycolytic activation in HSCs after 5-FU treatment and OXPHOS inhibition

bioRxiv preprint doi: https://doi.org/10.1101/2023.03.16.532898; this version posted March 18, 2023. The copyright holder for this preprint (which was not certified by peer review) is the author/funder, who has granted bioRxiv a license to display the preprint in perpetuity. It is made available under aCC-BY-NC-ND 4.0 International license.

could be demonstrated through unbiased mathematical simulations, we performed quantitative ^{13}C metabolic flux analysis (^{13}C-MFA). After generating a metabolic model for isotope labeling enrichment and setting appropriate lactate efflux values, a simulation was conducted using the labeled metabolite abundance data obtained from isotope tracer analysis. The appropriate lactate efflux for quiescent HSC (PBS-treated HSC) was determined to 65 after experimenting with values from 0–100. The lactate efflux of 5-FU- or oligomycin-treated HSCs was higher than that of quiescent HSCs based on the observation that labeled glycolytic metabolite levels were particularly elevated in *in vitro* tracer analysis (see "**Quantitative ^{13}C-MFA with OpenMebius**" under "**Supplementary Methods**" for more information). As a result, the variation in the flux values of all enzymatic reactions calculated in HSCs after 5-FU or oligomycin treatment became smaller compared to quiescent HSCs, suggesting that HSCs strictly regulated their metabolism in response to stress (Supplemental Figure 3A-C). Unlike PBS-treated HSCs, those treated with 5-FU or oligomycin exhibited preferential glycolytic activation rather than TCA- or PPP-based metabolic strategies; the first half of the glycolytic system appeared to be the site of metabolic activation (Figure 3A-D; Supplemental Figure 3D-U, Table S4). This increase in metabolic flux upstream of the glycolytic pathway was also supported by our *in vitro* tracer analysis (Figure 1B and Figure 2B), suggesting that ^{13}C-MFA was a valid metabolic simulation. Among the reactions in the first half of glycolysis, phosphorylation of fructose 6-phosphate by PFK is the irreversible and rate-limiting reaction[59]. A detailed review of *in vitro* isotope tracer analysis results showed that the ratio of fructose 1,6-bisphosphate (F1,6BP; the product of PFK) to F6P (the substrate of PFK) was greatly elevated in HSCs during proliferation and OXPHOS inhibition (Figure 3J-K). Together with the results of quantitative ^{13}C-MFA, these findings suggested that HSCs exhibit elevated glycolytic flux relative to mitochondrial activity by increasing PFK enzyme activity under various stress conditions.

HSCs under stress exhibit activation of glycolysis-initiated TCA cycle and NAS

To investigate the long-term glucose utilization of HSCs, we performed an *in vivo* tracer analysis with U-$^{13}C_6$ glucose based on recent reports[47,50] (Supplemental Figure 4A; see "**Preparation and storage of in vivo U-$^{13}C_6$-glucose tracer samples**" under "**Supplementary Methods**" for more information). In HSCs from 5-FU-treated mice, we observed increased labeling of glycolytic metabolites such as dihydroxyacetone phosphate, glycerol-3-phosphate, and phosphoenolpyruvate, as well as NAS metabolites such as inosine monophosphate and ATP, and those derived from TCA cycle such as aspartic acid and glutamate, compared to HSCs from PBS-treated mice (Supplemental

bioRxiv preprint doi: https://doi.org/10.1101/2023.03.16.532898; this version posted March 18, 2023. The copyright holder for this preprint (which was not certified by peer review) is the author/funder, who has granted bioRxiv a license to display the preprint in perpetuity. It is made available under aCC-BY-NC-ND 4.0 International license.

Figure 4B-I, Table S5). When the amount of U-$^{13}C_6$-glucose-derived labeled metabolites in each pathway was calculated, more glucose-derived metabolites entered TCA cycle in the 5-FU-treated group than PBS-treated group (Supplemental Figure 4J). Thus, although short-term (10–30 min) *in vitro* tracer analysis showed that HSCs exhibited more potent activation of anaerobic glycolysis than of other pathways in response to 5-FU administration, long-term (approx. 3 h) labeling by *in vivo* tracer analysis revealed that glycolysis-initiated TCA cycle and NAS flux were activated in addition to enhanced anaerobic glycolysis.

PFKFB3 accelerates glycolytic ATP production during HSC cell cycling

In vitro and *in vivo* tracer analysis results collectively suggested that the activation of glycolysis catalyzed by PFK may have been the starting point for the activation of the entire HSC metabolism. To analyze the contribution of PFK to ATP metabolism in steady-state or stressed HSCs, we needed to develop an experimental system that could measure the dynamics of ATP concentrations in HSCs in a non-destructive, real-time manner. To this end, we used knock-in GO-ATeam2 mice as a FRET-based biosensor of ATP concentration (see "**Time-course analysis of ATP levels in single hematopoietic cells using GO-ATeam2 system**" under "**Methods**" for more information.). The number of BMMNCs, as well as the frequency of HSCs ($CD150^+$CD48-LSK) and other progenitor cells, in the BM of GO-ATeam2$^+$ mice were almost unchanged compared to of C57B6/J mice, except for a mild decrease in the frequency of the Lin^- fraction (Supplementary Figure 5A-C). Using BMMNCs derived from GO-ATeam2$^+$ mice, we developed a method to detect changes in ATP concentration with high temporal resolution when the activity of PFK was modulated (**METHODS**, Supplemental Figure 5D-F). To validate our methods, we measured ATP concentrations in HSCs and MyPs with or without various nutrients (see "**Time-course analysis of FRET values**" under "**Supplementary Methods**" for more information.). MyPs showed more rapid decreases in ATP concentration than HSCs, suggesting higher ATP consumption by progenitors (Supplemental Figure 5G-H). Adding glucose to the medium suppressed this decrease in MyPs; however, other metabolites (e.g., pyruvate, lactate, and fatty acids) had minimal effects, suggesting that ATP levels are glycolysis-dependent in MyPs (Supplemental Figure 5G-H), consistent with previous reports that the aerobic glycolytic enzyme M2 pyruvate kinase isoform (PKM2) is required for progenitor cell function[33].

Further, we analyzed ATP consumption and metabolic dependency of cell-cycling HSCs after 5-FU administration (Figure 4A). After inhibiting glycolysis using 2-deoxy-D-glucose (2-DG)

bioRxiv preprint doi: https://doi.org/10.1101/2023.03.16.532898; this version posted March 18, 2023. The copyright holder for this preprint (which was not certified by peer review) is the author/funder, who has granted bioRxiv a license to display the preprint in perpetuity. It is made available under aCC-BY-NC-ND 4.0 International license.

with other mitochondrial substrates, 5-FU-treated HSCs showed more rapid decreases in ATP concentration than PBS-treated HSCs (Figure 4B-C). In contrast, OXPHOS inhibition by oligomycin without glucose or mitochondrial substrates decreased the ATP concentration to a similar extent in both 5-FU- and PBS-treated HSCs, although 5-FU-treated HSCs showed earlier ATP exhaustion (Figure 4D-E). These data suggest that 5-FU-treated-HSCs upregulated ATP production via glycolysis, rather than relying on mitochondria. Apoptosis assay revealed a slight increase in early apoptotic cells (annexin V^+ propidium iodide $[PI]^-$) after 2-DG treatment and a slight decrease in the number of viable cells (Annexin V^- PI^-) after oligomycin treatment, both to a very limited extent (approx. 5%) compared to the degree of ATP decrease, suggesting that the decrease in ATP after 2-DG or oligomycin treatment did not simply reflect cell death (Supplementary Figure 5I).

PFK is allosterically activated by 6-phosphofructo-2-kinase/fructose-2,6-bisphosphatase (PFKFB). Among the four isozymes of mammalian PFKFB, PFKFB3 is the most favorable for PFK activation[60]. We investigated whether PFKFB3 contributes to glycolytic plasticity in HSCs during proliferation. When treated with the PFKFB3 inhibitor AZ PFKFB3 26, compared with HSCs from PBS-treated mice, HSCs from 5-FU-treated mice showed decreased ATP levels (Figure 4F, H, Supplementary Figure 5J). Although AMPK activates PFKFB3 in other contexts[61], AMPK inhibition by dorsomorphin did not alter ATP concentration in 5-FU-treated-HSCs (Figure 4G, I).

OXPHOS inhibition accelerates glycolysis to sustain ATP levels in HSCs, but not in progenitors

To assess differences in metabolic dependence between steady-state or stressed and naturally proliferating HPCs, we altered ATP metabolism in HSCs and progenitors using 2-DG or oligomycin (Figure 5A). Oligomycin treatment rapidly depleted ATP in HSCs and all HPC fractions (green lines in Figure 5B-C; Supplemental Figure 6A-D). Treatment with 2-DG decreased ATP concentrations for a short amount of time (~12 min) in HSCs and HPCs, but ATP reduction was less evident than that induced by oligomycin (blue lines in Figure 5B-C; Supplemental Figure 6A-D). The ATP reduction induced by 2-DG treatment was particularly low (~15%) in HSCs, multipotent progenitor cells (MPPs), and common lymphoid progenitors (CLPs) relative to that in common myeloid progenitors (CMPs), granulocytes-macrophage progenitors (GMPs), and megakaryocyte-erythrocyte progenitors (MEPs) (Figure 5D).

Next, we investigated the role of glycolysis in ATP production during OXPHOS inhibition by combining oligomycin administration and glucose supplementation. ATP concentration remained more stable in HSCs treated with oligomycin and glucose than in those treated only with oligomycin.

bioRxiv preprint doi: https://doi.org/10.1101/2023.03.16.532898; this version posted March 18, 2023. The copyright holder for this preprint (which was not certified by peer review) is the author/funder, who has granted bioRxiv a license to display the preprint in perpetuity. It is made available under aCC-BY-NC-ND 4.0 International license.

Similar results were not seen in HPCs, indicating that HSCs have the plasticity to upregulate glycolytic ATP production to meet demands (orange lines in Figure 5B-C; Supplemental Figure 6A-D, summarized in Figure 5E). Similar to oligomycin treatment, rotenone (Complex I inhibitor) and carbonyl cyanide 4-(trifluoromethoxy)phenylhydrazone (FCCP, mitochondrial uncoupler) treatments, which inhibit OXPHOS-derived ATP production, also decreased ATP concentrations in HSCs, but not when administered simultaneously with glucose (Supplementary Figure 6E-F). Furthermore, with oligomycin, HSCs, but not HPCs, maintained ATP concentrations at low glucose levels (50 mg/dL) (Supplemental Figure 6G). These analyses suggest that ATP was produced by mitochondrial OXPHOS in steady-state HSCs, and that only HSCs, but not HPCs, maintained ATP production by glycolysis when OXPHOS was compromised.

PFKFB3 accelerates glycolytic ATP production during OXPHOS inhibition

Next, to understand whether PFKFB3 contributes to ATP production in HSCs under OXPHOS inhibition, we evaluated PFKFB3 function under OXPHOS inhibition using the GO-ATeam2^{+} BMMNCs. In oligomycin-treated HSCs, PFKFB3 inhibition led to rapidly decreased ATP concentration that was not observed in HSCs not treated with oligomycin (Figure 5F-I). We examined the effects of HSPC metabolic regulators on ATP levels in oligomycin-treated HSCs. Inhibiting PKM2, which accelerates glycolysis in steady-state progenitors[33], significantly reduced ATP levels in oligomycin-treated HSCs (Supplemental Figure 6H, J). Inhibiting LKB1, a kinase upstream of AMPK[62,63], did not affect the ATP concentration in oligomycin-treated HSCs (Supplemental Figure 6I, K), whereas levels of adenosine monophosphate (AMP), which also activates AMPK, increased in oligomycin-treated but not in 5-FU-treated HSCs (Supplemental Figure 6L). This may explain differences in AMPK-dependent ATP production between proliferative HSCs and HSCs under OXPHOS inhibition.

Next, we tested the effects of PFKFB3 on ATP concentration in HPCs. Unlike HSCs, HPCs exhibited PFKFB3-dependent ATP production, even without oligomycin (Supplemental Figure 6M-Q). Therefore, ATP production in steady-state HSCs was PFKFB3-independent, and proliferative stimulation or OXPHOS inhibition plastically activated glycolytic ATP production in a PFKFB3-dependent manner to meet ATP demand.

PFKFB3 activity renders HSCs dependent on glycolysis

Next, we investigated whether PFKFB3 activity itself confers glycolytic dependence on HSCs. We

bioRxiv preprint doi: https://doi.org/10.1101/2023.03.16.532898; this version posted March 18, 2023. The copyright holder for this preprint (which was not certified by peer review) is the author/funder, who has granted bioRxiv a license to display the preprint in perpetuity. It is made available under aCC-BY-NC-ND 4.0 International license.

retrovirally overexpressed *Pfkfb3* in HSCs and performed cell cycle analysis (Figure 5J). *Pfkfb3*-overexpressed HSCs increased the proportion of cells in the S/G2/M phase and decreased the number of G_0 cells compared to *mock*-overexpressed HSCs (Figure 5K). Next, we retrovirally overexpressed *Pfkfb3* in GO-ATeam2$^+$ HSCs and performed real-time ATP measurement (Figure 5J). *Pfkfb3*-overexpressing GO-ATeam2$^+$ HSCs did not show changes in ATP concentrations relative to those in *mock*-transduced cells (Figure 5L; Supplemental Figure 6R). Upon 2-DG treatment, *Pfkfb3*-overexpressing HSCs showed a greater decrease in ATP concentration than *mock*-transduced HSCs did (Figure 5M; Supplemental Figure 6S). However, oligomycin treatment of both *mock*-transduced and *Pfkfb3*-overexpressing HSCs decreased ATP concentration to comparable levels (Figure 5N; Supplemental Figure 6T). Notably, *Pfkfb3*-overexpressing HSCs recovered ATP levels more effectively under low glucose conditions (12.5 mg/dL) than did *mock*-transduced HSCs (Figure 5O; Supplemental Figure 6U). These data suggest that PFKFB3 directly conferred glycolytic dependence onto HSCs by modulating the cell cycle and increasing their ATP-generating capacity via glycolysis under metabolic stress.

PFKFB3 methylation by PRMT1 supports ATP production by cell-cycling HSCs

Next, we investigated how 5-FU-treated-HSCs regulate PFKFB3 independently of AMPK (Figure 4G, I). PFKFB3 activity is regulated at multiple levels[64], and PFKFB3 transcript and protein levels in HSCs remained unchanged during 5-FU-induced cell cycling (Figure 6A-B). Phosphorylation can also regulate PFKFB3 activity[61,65,66]; however, we observed no change in PFKFB3 phosphorylation in 5-FU-treated-HSCs (Figure 6C). Upon oligomycin exposure, PFKFB3 was phosphorylated by AMPK in the HSCs (Figure 6D). PFKFB3 is also methylated, and its activity is upregulated by protein arginine methyltransferase 1 (PRMT1)[67]. We observed that *Prmt1* expression increased in 5-FU-treated-HSCs relative to that in PBS-treated-HSCs (Figure 6E). Furthermore, PFKFB3 methylation was significantly induced in 5-FU-treated-HSCs than in PBS-treated-HSCs (Figure 6F). Treatment of HSCs with a PRMT1 inhibitor decreased PFKFB3 methylation (Figure 6G), suggesting that PRMT1 catalyzed PFKFB3 methylation. To investigate whether glycolytic activity in HSCs was regulated by m-PFKFB3, mice treated with PBS or 5-FU were injected with 2-NBDG, and m-PFKFB3 levels in HSCs with high and low 2-NBDG uptake were quantified. Regardless of PBS or 5-FU treatment, HSCs with high 2-NBDG uptake exhibited higher m-PFKFB3 levels than those with low uptake (Figure 6H), suggesting that m-PFKFB3 regulated the activity of the glycolytic system in HSCs.

bioRxiv preprint doi: https://doi.org/10.1101/2023.03.16.532898; this version posted March 18, 2023. The copyright holder for this preprint (which was not certified by peer review) is the author/funder, who has granted bioRxiv a license to display the preprint in perpetuity. It is made available under aCC-BY-NC-ND 4.0 International license.

Further, we analyzed the potential effects of PRMT1 inhibition on ATP concentration in GO-ATeam2^{+} HSCs. Treatment with the PRMT1 inhibitor significantly decreased ATP levels in 5-FU-treated-HSCs than in PBS-treated-HSCs (Figure 6I-J). These findings indicated that ATP levels in 5-FU-treated-HSCs were supported by PRMT1 methylation–mediated PFKFB3 activation.

PFKFB3 contributes to HSPC pool expansion and stress hematopoiesis maintenance

Finally, we analyzed PFKFB3 function in HSCs during hematopoiesis. We cultured HSCs with a PFKFB3 inhibitor *in vitro* under quiescence-maintaining or proliferative conditions (Supplementary Figure 7A)[68]. Cell count in HSC-derived colonies decreased following treatment with a PFKFB3 inhibitor under proliferative, but not quiescence-maintaining, conditions (Supplementary Figure 7B).

We also knocked out *Pfkfb3* in HSCs using the less toxic, vector-free CRISPR-Cas9 system and cultured the cells under quiescence-maintaining or proliferative conditions (Supplementary Figure 7A) based on recent reports by Shiroshita et al.[69]. Again, cell numbers in *Pfkfb3*-knockout (KO) HSC–derived colonies decreased only in proliferative cultures when compared to control cultures (*Rosa26*-KO HSCs) (Supplementary Figure 7C, E, F). We retrovirally overexpressed *Pfkfb3* in HSCs and cultured them under quiescence maintenance or proliferative conditions (Supplementary Figure 7A). *Pfkfb3*-overexpressing HSC colonies showed increased cell count compared to that of *mock*-transduced cells, but only under proliferative conditions (Supplementary Figure 7D).

To assess PFKFB3 function in HSCs *in vivo*, we transplanted *Pfkfb3*-KO HSCs (Ly5.2^{+}) or wild type (WT) control HSCs into lethally irradiated recipients (Ly5.1^{+}) as well as Ly5.1^{+} competitor cells (Figure 7A), and the behavior of *Pfkfb3*-KO cells was evaluated by Sanger sequencing of peripheral blood (PB) cells[69]. In the KO group, donor-derived chimerism in PB cells decreased relative to that in the WT control group during the early phase (1 month post-transplant) but recovered thereafter (Figure 7B). Next, we retrovirally transduced Ly5.2^{+} HSCs with *Pfkfb3* S461E (*Pfkfb3*CA), a constitutively active PFKFB3 mutant, and transplanted them into lethally irradiated recipients (Ly5.2^{+}), along with Ly5.1^{+} competitor cells (Figure 7A, Supplementary Figure 7G). Donor chimerism during the early post-transplant period in the *Pfkfb3*CA-overexpressing group was significantly higher than that in the *mock*-transduced group (Figure 7C). These findings suggested that PFKFB3 was required for differentiation and proliferation of HSCs to expand the HSPC pool. Therefore, we compared the contribution of PFKFB3 to HSPC function at steady state and after myeloproliferative stimulation. *Pfkfb3*- or *Rosa*-KO HSPCs were transplanted into recipients (Ly5.1^{+}). After 2 months, recipients received 5-FU intraperitoneally, and the dynamics of *Pfkfb3*- or

bioRxiv preprint doi: https://doi.org/10.1101/2023.03.16.532898; this version posted March 18, 2023. The copyright holder for this preprint (which was not certified by peer review) is the author/funder, who has granted bioRxiv a license to display the preprint in perpetuity. It is made available under aCC-BY-NC-ND 4.0 International license.

Rosa-KO cell abundance in PB was assessed (Figure 7D). In PB cells prior to 5-FU administration, *Pfkfb3*- or *Rosa*-KO HSPC-derived blood cells were almost equally present, suggesting that the loss of PFKFB3 did not affect steady-state blood cell production (Figure 7E). However, after 5-FU administration, *Pfkfb3*-KO HSPC-derived blood cell abundance was reduced compared to that in the *Rosa* group (Figure 7E). This change occurred on day 6 after 5-FU administration (day 1), when the cell cycle of HSCs was activated (Supplementary Figure 1B), suggesting that PFKFB3 served a function in the proliferation and differentiation of HSPCs from HSCs.

To investigate the mechanisms underlying the short-term effects of PFKFB3 on hematopoiesis after bone marrow transplantation (BMT), we evaluated cell cycle and apoptosis of *Pfkfb3*-KO or -overexpressing HSPCs on day 2 after BMT (Figure 7F). Cell cycle was analyzed by Ki67/Hoechst33432 staining and *in vivo* BrdU labeling [50], which showed that cell cycle progression was suppressed in *Pfkfb3*-KO HSPCs (Figure 7G-J). In contrast, *Pfkfb3* KO cells did not exhibit aberrant apoptosis of HSPCs after BMT (Figure 7K). Furthermore, we examined the cell cycle of HSPCs overexpressing *Pfkfb3*CA on day 2 after BMT (Figure 7L) and found that *Pfkfb3*CA-overexpressing HSPCs showed accelerated cell cycle compared to *mock*-overexpressing HSPCs (Figure 7M-N). These data indicate that PFKFB3 governs cell cycle progression and promotes the production of differentiated cells from HSCs in proliferative environments, both *in vitro* in the presence of cytokine stimulation and immediately after transplantation *in vivo*.

Discussion

In this study, by combining metabolomic tracing of U-$^{13}C_6$-labeled glucose and ^{13}C-MFA, we quantitatively identified the metabolic programs used by HSCs during steady-state, cell-cycling, and OXPHOS inhibition. Under proliferative stress, HSCs uniformly shift from mitochondrial respiration to glycolytic ATP production and PPP activation, which represent hallmarks of cell-cycling mammalian cells[70]. Previous reports have emphasized the importance of glycolysis in maintaining HSC quiescence, but have primarily analyzed HSCs in transplant assays, wherein HSCs must enter the cell cycle[32,71]. Prior analysis of repopulation capacity, which is positively correlated with enhanced glycolysis, may have overestimated glycolytic ATP production and overlooked mitochondrial ATP production during native hematopoiesis. In fact, some studies have suggested that OXPHOS activity is important for HSC maintenance and function[21].

Our method was based on recently reported quantitative metabolic analysis techniques for

bioRxiv preprint doi: https://doi.org/10.1101/2023.03.16.532898; this version posted March 18, 2023. The copyright holder for this preprint (which was not certified by peer review) is the author/funder, who has granted bioRxiv a license to display the preprint in perpetuity. It is made available under aCC-BY-NC-ND 4.0 International license.

very small numbers of cells[23,46-50], such as HSCs, and expands our knowledge of HSC metabolism during stress hematopoiesis. In our study, 5-FU administration in mice transiently decreased ATP concentration in HSCs in parallel with cell cycle progression, suggesting that HSC differentiation and cell cycle progression are closely related to intracellular metabolism and can be monitored by measuring ATP concentration. We mainly analyzed a mixture of $EPCR^+$ and $EPCR^-$ HSCs, and we believe that the observed cell cycle progression and promotion of glycolysis in both $EPCR^+$ and $EPCR^-$ HSCs support the validity of our claims (Figure 1J, Supplementary Figure 1F-J). According to ^{13}C-MFA enzymatic reaction flux of PFK in 5-FU-treated HSCs indicated a relative increase of approximately 10%. However, the flux value obtained by ^{13}C-MFA was calculated with glucose uptake as 100. Thus, when combined with the overall increase in the glycolytic pool demonstrated by *in vitro* isotopic glucose tracer analysis and *in vivo* NBDG analysis, rapid acceleration of glycolysis becomes evident throughout the HSCs, including subpopulations that were less responsive to stress[43-45]. These findings are consistent with reports suggesting that HSCs have relatively low biosynthetic activity[72,73] that is rapidly activated in response to cell proliferation stimuli[40,74]. Notably, we found that HSCs could accelerate glycolytic ATP production to fully compensate for mitochondrial ATP production under OXPHOS inhibition, a phenomenon that is difficult to identify without real-time ATP analysis. On the other hand, we observed that ATP production in steady-state or cell-cycling HSCs and in naturally proliferating HPCs depended more on mitochondrial OXPHOS than on glycolysis; inhibiting glycolysis in steady-state HSCs resulted in only mild ATP decreases. This is in contrast with the rapid decrease in ATP levels caused by OXPHOS inhibition. Because fatty acid β-oxidation is necessary for HSC self-renewal and quiescence[39,68], fatty acids may support mitochondrial ATP production independently of fluxes from glycolysis. Furthermore, although glycolysis and TCA cycle are decoupled in steady-state HSCs, in response to cell cycle progression, anaerobic glycolytic metabolism in HSCs is enhanced (Figure 1) and fluxes to TCA cycle and PPP from the glycolytic system are also promoted (Supplementary Figure 4). The difference in the degree of coupling between glycolysis and the TCA cycle between *in vitro* and *in vivo* tracer analysis may be explained by the difference in labeling time (10–30 min vs. 3 h). Altogether, these data provide direct evidence that glycolysis and TCA cycle become functionally uncoupled in quiescent HSCs[32,38]. Our findings are also consistent with previous reports of OXPHOS activation associated with HSC proliferation[32,36,75,76]. In other words, HSCs exhibit an increased proportion of anaerobic glycolysis–derived ATP by PFKFB3 upon proliferation and OXPHOS inhibition; furthermore, the glycolytic system is the starting point of metabolic activation and is indispensable for the overall enhancement

bioRxiv preprint doi: https://doi.org/10.1101/2023.03.16.532898; this version posted March 18, 2023. The copyright holder for this preprint (which was not certified by peer review) is the author/funder, who has granted bioRxiv a license to display the preprint in perpetuity. It is made available under aCC-BY-NC-ND 4.0 International license.

of HSC metabolism (Figure 7H).

HPCs and leukemic cells accelerate glycolytic ATP production using PKM2 for differentiation and transformation, respectively[33]; however, we demonstrated that glycolytic acceleration does not fully compensate for mitochondrial ATP production in HPCs. Mechanistically, PFKFB3 increased glycolytic activity in HSCs to maintain ATP concentrations during proliferation and OXPHOS inhibition. Under steady-state conditions, naturally proliferating HPCs rely on PFKFB3 for ATP production, whereas HSCs do not. Therefore, we can infer that quiescent HSCs at steady state can produce ATP via PFKFB3 activation in response to stress, enabling ATP generation. Furthermore, overexpression of *Pfkfb3* in HSCs increased glycolytic dependency, suggesting that PFKFB3 itself can modulate metabolic dependency in HSCs. Changes in glycolytic dependency in HSCs overexpressing *Pfkfb3* may seem small (0.06–0.13 mM) (Figure 5M, O). However, it is noteworthy that the rate of the reaction catalyzed by PFK varies greatly within a very narrow range of ATP concentrations, less than 1 mM. Webb et al. analyzed the factors controlling PFK activity and reported that the reaction rate of PFK varies by approximately 40% in the 0.3–1 mM ATP concentration range[77]. The reason that differences in glycolytic dependence could be detected in cells overexpressing *Pfkfb3* may be that the ATP concentration at the time of analysis was approximately 0.5–0.6 mM, which is within the range where a small change in ATP concentration can dynamically alter PFK activity.

PFKFB3 supports hematopoiesis in contexts that require robust HSPC proliferation *in vitro* and *in vivo*. We showed that the positive or negative effect of *Pfkfb3* overexpression or KO on differentiated blood cell production is gradually lost after BMT. This is because HSPCs require PFKFB3 for cell cycle progression during stress hematopoiesis in the early phase after BMT (Figure 7F-J, and L-N). However, HSCs no longer require PFKFB3 for a certain period of time after BMT, probably because they regain a quiescent state. This is consistent with the fact that inhibition of PFKFB3 in quiescent HSCs does not reduce the ATP concentration (Figure 5F, H), suggesting that the activity of PFKFB3 is plastically modified. HSC metabolic plasticity is also illustrated by the mode of PFKFB3 activation, differing depending on stress type. During proliferative stress, PRMT1 methylates PFKFB3 in the HSCs to promote glycolytic ATP production, a modification that increases its activity[67]. PRMT1 is required for stress hematopoiesis[78], but its downstream targets in HSCs remain unclear. Our results strongly suggest that PRMT1 targets PFKFB3 to stimulate glycolysis in HSCs. In contrast, under OXPHOS inhibition, PFKFB3 phosphorylation by AMPK is induced—another modification that also upregulates its activity. These two PFKFB3 protein modifications

bioRxiv preprint doi: https://doi.org/10.1101/2023.03.16.532898; this version posted March 18, 2023. The copyright holder for this preprint (which was not certified by peer review) is the author/funder, who has granted bioRxiv a license to display the preprint in perpetuity. It is made available under aCC-BY-NC-ND 4.0 International license.

allow for flexible regulation of ATP production by glycolysis, even under simultaneous and different stresses. In fact, the constitutively active S461E PFKFB3 mutant, designed to mimic phosphorylation in response to OXPHOS inhibition, enhanced HSC reconstitution capacity after transplantation, suggesting that even if PFKFB3 is activated by one stress (in this case, proliferative), it has the activation capacity to respond to a different stress (i.e., mitochondrial). Therefore, the functions of phosphorylated and methylated forms of PFKFB3 are to some extent interchangeable, and either modification can be used to handle diverse stresses.

In summary, we found that HSCs exhibit a highly dynamic range of glycolytic flux. Our study highlights glycolysis as a pivotal source of energy production in stressed HSCs, and indicates that OXPHOS, although an important source of ATP, can be uncoupled from glycolysis in steady-state HSCs without compromising ATP levels. Because multiple PFKFB3 modifications safeguard HSCs against different stresses by accelerating glycolysis, interventions targeting these might effectively induce or manage stress hematopoiesis. This study provides a platform for comprehensive and quantitative real-time analysis of ATP concentration and its dynamics in HSPCs. Our approach allows for analysis of metabolic programs in rare cells and detection of various metabolic activities within a diverse cell population, making it applicable to the analysis of various tissue systems in normal and diseased states.

Acknowledgments

We thank E. Lamar for preparation of the manuscript, T. Kitamura for providing mVenus-p27K- mice, and N. Toyama-Sorimachi and H. Shindou for their critical reading of the manuscript. This work was supported in part by KAKENHI grants from MEXT/JSPS (JP19K17847 to H.K.; JP19K17877, JP21J01690 to D.K.; JP18H02845, JP20K21621, JP21H02957 to K.T.), AMED grants (JP22zf0127007 to M.S.; JP18ck0106444, JP18ae0201014, JP20bm0704042, JP20gm1210011 to K.T.), grants from the National Center for Global Health and Medicine (29-1015, 20A1010 to H.K.; 26-001, 21A2001 to K.T.), the Takeda Science Foundation (to D.K. and K.T.), a JB Research Grant (to D.K.), the Human Biology Microbiome Quantum Research Center (WPI-Bio2Q) supported by MEXT (to M.S.), and the MEXT Joint Usage/Research Center Program at the Advanced Medical Research Center, Yokohama City University (to K.T.).

Author Contributions

S.W., H.K., Y. Sugiura, M.Y., K.S., Y. Sorimachi, D.K., S.K., M.O., A.N., K.M., M.H., and S.T.

bioRxiv preprint doi: https://doi.org/10.1101/2023.03.16.532898; this version posted March 18, 2023. The copyright holder for this preprint (which was not certified by peer review) is the author/funder, who has granted bioRxiv a license to display the preprint in perpetuity. It is made available under aCC-BY-NC-ND 4.0 International license.

600 performed the study and analyzed data; T. Yamamoto, T. Yabushita, Y.T, H.H., S.O., N.G., T.T., A.N-
601 I., M.S., A.I., T.S., and K.T. provided scientific advice and materials; S.W., H. K., A.N-I. and K.T.
602 wrote the manuscript; and K.T. conceived the project and supervised the research.
603
604 **Conflict of interest**
605 The authors declare no competing financial interests.
606
607 **References**
608 1. Schirmer T, Evans PR. Structural basis of the allosteric behaviour of phosphofructokinase. *Nature*.
609 1990;343(6254):140-145.
610 2. Denton RM, Randle PJ, Bridges BJ, et al. Regulation of mammalian pyruvate dehydrogenase. *Mol Cell*
611 *Biochem*. 1975;9(1):27-53.
612 3. Harris RA, Hawes JW, Popov KM, et al. Studies on the regulation of the mitochondrial alpha-ketoacid
613 dehydrogenase complexes and their kinases. *Adv Enzyme Regul*. 1997;37:271-293.
614 4. Sols A. Multimodulation of enzyme activity. *Curr Top Cell Regul*. 1981;19:77-101.
615 5. Gabriel JL, Milner R, Plaut GW. Inhibition and activation of bovine heart NAD-specific isocitrate
616 dehydrogenase by ATP. *Arch Biochem Biophys*. 1985;240(1):128-134.
617 6. Frieden C. Glutamate Dehydrogenase. Vi. Survey of Purine Nucleotide and Other Effects on the Enzyme from
618 Various Sources. *J Biol Chem*. 1965;240:2028-2035.
619 7. Hardie DG, Ross FA, Hawley SA. AMPK: a nutrient and energy sensor that maintains energy homeostasis. *Nat*
620 *Rev Mol Cell Biol*. 2012;13(4):251-262.
621 8. Lin SC, Hardie DG. AMPK: Sensing Glucose as well as Cellular Energy Status. *Cell Metab*. 2018;27(2):299-
622 313.
623 9. Hardie DG, Carling D. The AMP-activated protein kinase--fuel gauge of the mammalian cell? *Eur J Biochem*.
624 1997;246(2):259-273.
625 10. Pinho S, Frenette PS. Haematopoietic stem cell activity and interactions with the niche. *Nat Rev Mol Cell Biol*.
626 2019;20(5):303-320.
627 11. Crane GM, Jeffery E, Morrison SJ. Adult haematopoietic stem cell niches. *Nat Rev Immunol*. 2017;17(9):573-
628 590.
629 12. de Haan G, Lazare SS. Aging of hematopoietic stem cells. *Blood*. 2018;131(5):479-487.
630 13. Mejia-Ramirez E, Florian MC. Understanding intrinsic hematopoietic stem cell aging. *Haematologica*.
631 2020;105(1):22-37.
632 14. Orkin SH, Zon LI. Hematopoiesis: an evolving paradigm for stem cell biology. *Cell*. 2008;132(4):631-644.
633 15. Nakada D, Saunders TL, Morrison SJ. Lkb1 regulates cell cycle and energy metabolism in haematopoietic
634 stem cells. *Nature*. 2010;468(7324):653-658.
635 16. Gurumurthy S, Xie SZ, Alagesan B, et al. The Lkb1 metabolic sensor maintains haematopoietic stem cell

bioRxiv preprint doi: https://doi.org/10.1101/2023.03.16.532898; this version posted March 18, 2023. The copyright holder for this preprint (which was not certified by peer review) is the author/funder, who has granted bioRxiv a license to display the preprint in perpetuity. It is made available under aCC-BY-NC-ND 4.0 International license.

636 survival. *Nature*. 2010;468(7324):659-663.
637 17. Gan B, Hu J, Jiang S, et al. Lkb1 regulates quiescence and metabolic homeostasis of haematopoietic stem cells.
638 *Nature*. 2010;468(7324):701-704.
639 18. Sahin E, Colla S, Liesa M, et al. Telomere dysfunction induces metabolic and mitochondrial compromise.
640 *Nature*. 2011;470(7334):359-365.
641 19. Luchsinger LL, de Almeida MJ, Corrigan DJ, Mumau M, Snoeck HW. Mitofusin 2 maintains haematopoietic
642 stem cells with extensive lymphoid potential. *Nature*. 2016;529(7587):528-531.
643 20. de Almeida MJ, Luchsinger LL, Corrigan DJ, Williams LJ, Snoeck HW. Dye-Independent Methods Reveal
644 Elevated Mitochondrial Mass in Hematopoietic Stem Cells. *Cell Stem Cell*. 2017;21(6):725-729.e724.
645 21. Anso E, Weinberg SE, Diebold LP, et al. The mitochondrial respiratory chain is essential for haematopoietic
646 stem cell function. *Nat Cell Biol*. 2017;19(6):614-625.
647 22. Nakamura-Ishizu A, Matsumura T, Stumpf PS, et al. Thrombopoietin Metabolically Primes Hematopoietic
648 Stem Cells to Megakaryocyte-Lineage Differentiation. *Cell Rep*. 2018;25(7):1772-1785 e1776.
649 23. Qi L, Martin-Sandoval MS, Merchant S, et al. Aspartate availability limits hematopoietic stem cell function
650 during hematopoietic regeneration. *Cell Stem Cell*. 2021;28(11):1982-1999 e1988.
651 24. Filippi MD, Ghaffari S. Mitochondria in the maintenance of hematopoietic stem cells: new perspectives and
652 opportunities. *Blood*. 2019;133(18):1943-1952.
653 25. Guitart AV, Panagopoulou TI, Villacreces A, et al. Fumarate hydratase is a critical metabolic regulator of
654 hematopoietic stem cell functions. *J Exp Med*. 2017;214(3):719-735.
655 26. Hsu P, Qu CK. Metabolic plasticity and hematopoietic stem cell biology. *Curr Opin Hematol*. 2013;20(4):289-
656 294.
657 27. Busch K, Klapproth K, Barile M, et al. Fundamental properties of unperturbed haematopoiesis from stem cells
658 in vivo. *Nature*. 2015;518(7540):542-546.
659 28. Sun J, Ramos A, Chapman B, et al. Clonal dynamics of native haematopoiesis. *Nature*. 2014;514(7522):322-
660 327.
661 29. Ho TT, Warr MR, Adelman ER, et al. Autophagy maintains the metabolism and function of young and old
662 stem cells. *Nature*. 2017;543(7644):205-210.
663 30. Laurenti E, Gottgens B. From haematopoietic stem cells to complex differentiation landscapes. *Nature*.
664 2018;553(7689):418-426.
665 31. Nakamura-Ishizu A, Ito K, Suda T. Hematopoietic Stem Cell Metabolism during Development and Aging. *Dev*
666 *Cell*. 2020;54(2):239-255.
667 32. Takubo K, Nagamatsu G, Kobayashi CI, et al. Regulation of glycolysis by Pdk functions as a metabolic
668 checkpoint for cell cycle quiescence in hematopoietic stem cells. *Cell Stem Cell*. 2013;12(1):49-61.
669 33. Wang YH, Israelsen WJ, Lee D, et al. Cell-state-specific metabolic dependency in hematopoiesis and
670 leukemogenesis. *Cell*. 2014;158(6):1309-1323.
671 34. Simsek T, Kocabas F, Zheng J, et al. The distinct metabolic profile of hematopoietic stem cells reflects their
672 location in a hypoxic niche. *Cell Stem Cell*. 2010;7(3):380-390.

bioRxiv preprint doi: https://doi.org/10.1101/2023.03.16.532898; this version posted March 18, 2023. The copyright holder for this preprint (which was not certified by peer review) is the author/funder, who has granted bioRxiv a license to display the preprint in perpetuity. It is made available under aCC-BY-NC-ND 4.0 International license.

673 35. Inoue S, Noda S, Kashima K, Nakada K, Hayashi J, Miyoshi H. Mitochondrial respiration defects modulate
674 differentiation but not proliferation of hematopoietic stem and progenitor cells. *FEBS Lett*. 2010;584(15):3402-3409.
675 36. Yu WM, Liu X, Shen J, et al. Metabolic regulation by the mitochondrial phosphatase PTPMT1 is required for
676 hematopoietic stem cell differentiation. *Cell Stem Cell*. 2013;12(1):62-74.
677 37. Bejarano-Garcia JA, Millan-Ucles A, Rosado IV, et al. Sensitivity of hematopoietic stem cells to mitochondrial
678 dysfunction by SdhD gene deletion. *Cell Death Dis*. 2016;7(12):e2516.
679 38. Halvarsson C, Eliasson P, Jonsson JI. Pyruvate dehydrogenase kinase 1 is essential for transplantable mouse
680 bone marrow hematopoietic stem cell and progenitor function. *PLoS One*. 2017;12(2):e0171714.
681 39. Ito K, Carracedo A, Weiss D, et al. A PML–PPAR-δ pathway for fatty acid oxidation regulates hematopoietic
682 stem cell maintenance. *Nat Med*. 2012;18(9):1350-1358.
683 40. Karigane D, Kobayashi H, Morikawa T, et al. p38α Activates Purine Metabolism to Initiate Hematopoietic
684 Stem/Progenitor Cell Cycling in Response to Stress. *Cell Stem Cell*. 2016;19(2):192-204.
685 41. Umemoto T, Johansson A, Ahmad SAI, et al. ATP citrate lyase controls hematopoietic stem cell fate and
686 supports bone marrow regeneration. *EMBO J*. 2022:e109463.
687 42. Liang R, Arif T, Kalmykova S, et al. Restraining Lysosomal Activity Preserves Hematopoietic Stem Cell
688 Quiescence and Potency. *Cell Stem Cell*. 2020;26(3):359-376 e357.
689 43. Bowling S, Sritharan D, Osorio FG, et al. An Engineered CRISPR-Cas9 Mouse Line for Simultaneous
690 Readout of Lineage Histories and Gene Expression Profiles in Single Cells. *Cell*. 2020;181(6):1410-1422 e1427.
691 44. Fanti AK, Busch K, Greco A, et al. Flt3- and Tie2-Cre tracing identifies regeneration in sepsis from
692 multipotent progenitors but not hematopoietic stem cells. *Cell Stem Cell*. 2023;30(2):207-218 e207.
693 45. Munz CM, Dressel N, Chen M, Grinenko T, Roers A, Gerbaulet A. Regeneration following blood loss and
694 acute inflammation proceeds without contribution of primitive HSCs. *Blood*. 2023.
695 46. Agathocleous M, Meacham CE, Burgess RJ, et al. Ascorbate regulates haematopoietic stem cell function and
696 leukaemogenesis. *Nature*. 2017;549(7673):476-481.
697 47. DeVilbiss AW, Zhao Z, Martin-Sandoval MS, et al. Metabolomic profiling of rare cell populations isolated by
698 flow cytometry from tissues. *Elife*. 2021;10.
699 48. Lengefeld J, Cheng CW, Maretich P, et al. Cell size is a determinant of stem cell potential during aging. *Sci*
700 *Adv*. 2021;7(46):eabk0271.
701 49. Schonberger K, Obier N, Romero-Mulero MC, et al. Multilayer omics analysis reveals a non-classical retinoic
702 acid signaling axis that regulates hematopoietic stem cell identity. *Cell Stem Cell*. 2022;29(1):131-148 e110.
703 50. Jun S, Mahesula S, Mathews TP, et al. The requirement for pyruvate dehydrogenase in leukemogenesis
704 depends on cell lineage. *Cell Metab*. 2021;33(9):1777-1792 e1778.
705 51. Imamura H, Nhat KP, Togawa H, et al. Visualization of ATP levels inside single living cells with fluorescence
706 resonance energy transfer-based genetically encoded indicators. *Proc Natl Acad Sci U S A*. 2009;106(37):15651-15656.
707 52. Nakano M, Imamura H, Nagai T, Noji H. Ca(2)(+) regulation of mitochondrial ATP synthesis visualized at the
708 single cell level. *ACS Chem Biol*. 2011;6(7):709-715.
709 53. Yamamoto M, Kim M, Imai H, Itakura Y, Ohtsuki G. Microglia-Triggered Plasticity of Intrinsic Excitability

bioRxiv preprint doi: https://doi.org/10.1101/2023.03.16.532898; this version posted March 18, 2023. The copyright holder for this preprint (which was not certified by peer review) is the author/funder, who has granted bioRxiv a license to display the preprint in perpetuity. It is made available under aCC-BY-NC-ND 4.0 International license.

Modulates Psychomotor Behaviors in Acute Cerebellar Inflammation. *Cell Rep*. 2019;28(11):2923-2938 e2928.

54. Oki T, Nishimura K, Kitaura J, et al. A novel cell-cycle-indicator, mVenus-p27K-, identifies quiescent cells and visualizes G0-G1 transition. *Sci Rep*. 2014;4:4012.

55. Fukushima T, Tanaka Y, Hamey FK, et al. Discrimination of Dormant and Active Hematopoietic Stem Cells by G0 Marker Reveals Dormancy Regulation by Cytoplasmic Calcium. *Cell Rep*. 2019;29(12):4144-4158 e4147.

56. Miyajima M, Zhang B, Sugiura Y, et al. Metabolic shift induced by systemic activation of T cells in PD-1-deficient mice perturbs brain monoamines and emotional behavior. *Nat Immunol*. 2017;18(12):1342-1352.

57. Arai F, Hirao A, Ohmura M, et al. Tie2/angiopoietin-1 signaling regulates hematopoietic stem cell quiescence in the bone marrow niche. *Cell*. 2004;118(2):149-161.

58. Miller I, Min M, Yang C, et al. Ki67 is a Graded Rather than a Binary Marker of Proliferation versus Quiescence. *Cell Rep*. 2018;24(5):1105-1112 e1105.

59. Dunaway GA. A review of animal phosphofructokinase isozymes with an emphasis on their physiological role. *Mol Cell Biochem*. 1983;52(1):75-91.

60. Yalcin A, Telang S, Clem B, Chesney J. Regulation of glucose metabolism by 6-phosphofructo-2-kinase/fructose-2,6-bisphosphatases in cancer. *Exp Mol Pathol*. 2009;86(3):174-179.

61. Marsin AS, Bouzin C, Bertrand L, Hue L. The stimulation of glycolysis by hypoxia in activated monocytes is mediated by AMP-activated protein kinase and inducible 6-phosphofructo-2-kinase. *J Biol Chem*. 2002;277(34):30778-30783.

62. Hardie DG. AMPK--sensing energy while talking to other signaling pathways. *Cell Metab*. 2014;20(6):939-952.

63. Long YC, Zierath JR. AMP-activated protein kinase signaling in metabolic regulation. *J Clin Invest*. 2006;116(7):1776-1783.

64. Shi L, Pan H, Liu Z, Xie J, Han W. Roles of PFKFB3 in cancer. *Signal Transduct Target Ther*. 2017;2:17044.

65. Novellasdemunt L, Bultot L, Manzano A, et al. PFKFB3 activation in cancer cells by the p38/MK2 pathway in response to stress stimuli. *Biochem J*. 2013;452(3):531-543.

66. Okamura N, Sakakibara R. A common phosphorylation site for cyclic AMP-dependent protein kinase and protein kinase C in human placental 6-phosphofructo-2-kinase/fructose-2,6-bisphosphatase. *Biosci Biotechnol Biochem*. 1998;62(10):2039-2042.

67. Yamamoto T, Takano N, Ishiwata K, et al. Reduced methylation of PFKFB3 in cancer cells shunts glucose towards the pentose phosphate pathway. *Nat Commun*. 2014;5:3480.

68. Kobayashi H, Morikawa T, Okinaga A, et al. Environmental Optimization Enables Maintenance of Quiescent Hematopoietic Stem Cells Ex Vivo. *Cell Rep*. 2019;28(1):145-158 e149.

69. Shiroshita K, Kobayashi H, Watanuki S, et al. A culture platform to study quiescent hematopoietic stem cells following genome editing. *Cell Rep Methods*. 2022;2(12):100354.

70. Intlekofer AM, Finley LWS. Metabolic signatures of cancer cells and stem cells. *Nat Metab*. 2019;1(2):177-188.

71. Takubo K, Goda N, Yamada W, et al. Regulation of the HIF-1alpha level is essential for hematopoietic stem

bioRxiv preprint doi: https://doi.org/10.1101/2023.03.16.532898; this version posted March 18, 2023. The copyright holder for this preprint (which was not certified by peer review) is the author/funder, who has granted bioRxiv a license to display the preprint in perpetuity. It is made available under aCC-BY-NC-ND 4.0 International license.

cells. *Cell Stem Cell*. 2010;7(3):391-402.

72. Signer RA, Magee JA, Salic A, Morrison SJ. Haematopoietic stem cells require a highly regulated protein synthesis rate. *Nature*. 2014;509(7498):49-54.

73. Essers MA, Offner S, Blanco-Bose WE, et al. IFNalpha activates dormant haematopoietic stem cells in vivo. *Nature*. 2009;458(7240):904-908.

74. Umemoto T, Hashimoto M, Matsumura T, Nakamura-Ishizu A, Suda T. Ca(2+)-mitochondria axis drives cell division in hematopoietic stem cells. *J Exp Med*. 2018;215(8):2097-2113.

75. Maryanovich M, Zaltsman Y, Ruggiero A, et al. An MTCH2 pathway repressing mitochondria metabolism regulates haematopoietic stem cell fate. *Nat Commun*. 2015;6:7901.

76. Ito K, Carracedo A, Weiss D, et al. A PML-PPAR-delta pathway for fatty acid oxidation regulates hematopoietic stem cell maintenance. *Nat Med*. 2012;18(9):1350-1358.

77. Webb BA, Forouhar F, Szu FE, Seetharaman J, Tong L, Barber DL. Structures of human phosphofructokinase-1 and atomic basis of cancer-associated mutations. *Nature*. 2015;523(7558):111-114.

78. Zhu L, He X, Dong H, et al. Protein arginine methyltransferase 1 is required for maintenance of normal adult hematopoiesis. *Int J Biol Sci*. 2019;15(13):2763-2773.

bioRxiv preprint doi: https://doi.org/10.1101/2023.03.16.532898; this version posted March 18, 2023. The copyright holder for this preprint (which was not certified by peer review) is the author/funder, who has granted bioRxiv a license to display the preprint in perpetuity. It is made available under aCC-BY-NC-ND 4.0 International license.

Figure Legends

Figure 1. HSC cell cycling increases overall glycolytic flux, but not flux into mitochondria.

(A) Experimental design used for glucose isotope tracer analysis in HSCs from 5-FU- or PBS-treated mice. **(B)** Heat map of metabolite levels in HSCs derived from mice treated with PBS or 5-FU. **(C-F)** Relative amounts of U-$^{13}C_6$-glucose-derived metabolites in glycolysis (C), the first round of TCA cycle (D), the PPP €, and nucleotide synthesis (F) in HSCs from 5-FU- or PBS-treated mice (PBS group = 1.0); In (B)-(F), biological replicates from the PBS and 5-FU groups, obtained on three separate days, were pooled, analyzed by IC-MS, quantified based on calibration curve data for each metabolite (see "**Ion chromatography mass spectrometry (IC-MS) analysis**" section in "**Methods**" for details). **(G)** Experimental schema of *in vivo* 2-NBDG analysis. **(H)** Representative histograms of 2-NBDG analysis (gray: no 2-NBDG, red: PBS group, blue: 5-FU group). **(I)** 2-NBDG positivity in each fraction; data represent four pooled biological replicates for the PBS group and three for the 5-FU group; MyP: myeloid progenitor. **(J)** EPCR expression and 2-NBDG positivity within HSC fractions. Data were extracted from each individual in (I).

Data are presented as mean ± SD. * $p \leq 0.05$, ** $p \leq 0.01$, *** $p \leq 0.001$ as determined by paired-samples *t*-test (C-F) and Student's *t*-test (I and J). Abbreviations: G6P, glucose-6-phosphate; F6P, fructose-6-phosphate; F1,6BP, fructose-1,6-bisphosphate; G3P, glycerol-3-phosphate; DHAP, dihydroxyacetone phosphate; 3PG, 3-phosphoglycerate; 2PG, 2-phosphoglycerate; PEP, phosphoenolpyruvate; PYR, pyruvate; LAC, lactate; Ac-CoA; acetyl-CoA; CIT, citrate; ACO, cis-aconitic acid, isocitrate; 2OG, 2-oxoglutarate; SUC, succinate; FUM, fumarate; MAL, malate; OAA, oxaloacetate; 6PG, glucose-6-phosphate; Ru5P, ribulose-5-phosphate; Xu5P, xylulose-5-phosphate; R5P, ribose-5-phosphate; S7P, sedoheptulose-7-phosphate; E4P, erythrose-4-phosphate; PRPP, phosphoribosyl pyrophosphate; IMP, inosine monophosphate; ATP, adenosine triphosphate; GTP, guanine triphosphate; UMP, uridine monophosphate; UTP, uridine triphosphate; TTP, thymidine triphosphate. See also Fig. S1 and S2.

Figure 2. OXPHOS inhibition activates compensatory glycolysis in HSCs.

(A) Experimental design used for glucose isotope tracer analysis in HSCs treated with the OXPHOS inhibitor oligomycin. **(B)** Heat map of metabolite levels detected by *in vitro* tracer analysis of U-$^{13}C_6$-glucose in HSCs treated with DMSO or oligomycin (Oligo). **(C-F)** Relative amounts of U-$^{13}C_6$-glucose-derived metabolites in glycolysis (C), the first round of TCA cycle (D), the P€(E), and nucleotide synthesis (F) in DMSO- (black) or oligomycin-treated (orange) HSCs; In (B)-(F),

bioRxiv preprint doi: https://doi.org/10.1101/2023.03.16.532898; this version posted March 18, 2023. The copyright holder for this preprint (which was not certified by peer review) is the author/funder, who has granted bioRxiv a license to display the preprint in perpetuity. It is made available under aCC-BY-NC-ND 4.0 International license.

biological replicates of the DMSO and oligomycin groups obtained on four separate days were pooled, analyzed by IC-MS, and quantified based on calibration curve data for each metabolite (see "**Ion chromatography mass spectrometry (IC-MS) analysis**" section in "**Methods**" for details). (G-H) Overview of the Mito Stress test on the Seahorse flux analyzer for HSC and MyPs; (G) ECAR before and after oligomycin treatment (H). (Data were obtained from n = 3 technical replicates for HSCs and n = 10 technical replicates for MyPs.)

Data are shown as mean ± SD. * $p \leq 0.05$, ** $p \leq 0.01$, *** $p \leq 0.001$ as determined by paired-samples t-test (C-E) and Student's *t*-test (H). Abbreviations: G6P, glucose-6-phosphate; F6P, fructose-6-phosphate; F1,6BP, fructose-1,6-bisphosphate; G3P, glycerol-3-phosphate; DHAP, dihydroxyacetone phosphate; 3PG, 3-phosphoglycerate; 2PG, 2-phosphoglycerate; PEP, phosphoenolpyruvate; PYR, pyruvate; LAC, lactate; Ac-CoA; acetyl-CoA; CIT, citrate; ACO, cis-aconitic acid, isocitrate; 2OG, 2-oxoglutarate; SUC, succinate; FUM, fumarate; MAL, malate; OAA, oxaloacetate; 6PG, glucose-6-phosphate; Ru5P, ribulose-5-phosphate; Xu5P, xylulose-5-phosphate; R5P, ribose-5-phosphate; S7P, sedoheptulose-7-phosphate; E4P, erythrose-4-phosphate; PRPP, phosphoribosyl pyrophosphate; IMP, inosine monophosphate; ATP, adenosine triphosphate; GTP, guanine triphosphate; UMP, uridine monophosphate; UTP, uridine triphosphate; TTP, thymidine triphosphate. See also Fig. S2.

Figure 3. Quantitative ^{13}C-MFA of quiescent, proliferative, and stressed HSCs

(A-C) Overview of quantitative ^{13}C-MFA of PBS-treated HSCs (A), 5-FU-treated HSCs (B), and OXPHOS-inhibited HSCs (C). The representative net flux for each reaction with glucose uptake as 100 is shown in the squares below the catalytic enzymes for each reaction listed in green letters. Red arrows indicate reactions with particularly elevated fluxes and blue arrows indicate reactions with particularly decreased fluxes. (D) Heatmap of the relative flux of each enzyme in the 5-FU or oligomycin groups compared to that in the quiescent (Ctl) HSC (The metabolic flux of each enzyme in the Ctl group was standardized as 100.). **(E-J)** Fluxes due to reactions with PFK (E, H), G6PD (F, I), and PDH (G, J). Fluxes of HSCs derived from mice treated with 5-FU (blue bars) or PBS (red bars) (D-F) and of HSCs treated with DMSO (black bars) or oligomycin (orange bars) (G-I) are shown. Data is obtained from 100 simulations in OpenMebius, and flux data for each enzyme is displayed (Table S4). **(K-L)** Ratio of fructose 1,6-bisphosphate (F1,6BP) to fructose-6-phosphate (F6P) calculated from tracer experiments shown in Figure 1B and Figure 2B. Effects of 5-FU administration (K) or mitochondrial inhibition by oligomycin (L) are summarized. Data are shown as

bioRxiv preprint doi: https://doi.org/10.1101/2023.03.16.532898; this version posted March 18, 2023. The copyright holder for this preprint (which was not certified by peer review) is the author/funder, who has granted bioRxiv a license to display the preprint in perpetuity. It is made available under aCC-BY-NC-ND 4.0 International license.

mean ± SD. * p ≤ 0.05, ** p ≤ 0.01, *** p ≤ 0.001 as determined by Student's *t*-test (E-L). Abbreviations: HK, hexokinase; PGI, glucose-6-phosphate isomerase; PFK, phosphofructokinase; TPI, triose phosphate isomerase; GAPDH, glyceraldehyde-3-phosphate dehydrogenase; PGM, phosphoglycerate mutase; PK, pyruvate kinase; LDH, lactate dehydrogenase; PC, pyruvate carboxylase; PDH, pyruvate dehydrogenase; CS; citrate synthase; IDH, isocitrate dehydrogenase; αKGDH, α-ketoglutaric acid dehydrogenase; SDH, succinate dehydrogenase; G6PD, glucose-6-phosphate dehydrogenase; TAL, transaldolase. See also Fig. S3.

Figure 4. Pfkfb3 activates the glycolytic system in proliferating HSCs

(A) Experimental design used to conduct real-time ATP analysis of HSCs treated with 5-FU or PBS. PLFA medium containing mitochondrial substrates (pyruvate, lactate, fatty acids, and amino acids) but no glucose, was used for experiments with 2-DG; Ba-M containing neither mitochondrial substrates nor glucose was used for experiments with oligomycin, Pfkfb3 inhibitor, or AMPK inhibitor. **(B-I)** Results of real-time ATP analysis of PBS- (red) or 5-FU-treated (blue) HSCs after treatment with 2-DG (B, D), oligomycin (C, E), PFKFB3 inhibitor (F, H), or AMPK inhibitor (G, I). Bar graphs show corrected ATP concentrations for the last 2 min (D) of (B), 6–7 min (E) of (C), or the last 1 min (H, I) of (F, G) for PFKFB3 and AMPK inhibitors, respectively. Each group represents at least 60 cells. Data are representative results of pooled samples from three biological replicates. (see "**Time-course analysis of FRET values**" in "**Supplementary Methods**" for details of the correction method used to calculate ATP concentration.)

Data are presented as mean ± SD. * p ≤ 0.05, ** p ≤ 0.01, *** p ≤ 0.001 as determined by Student's *t*-test (D, E, H, and I). See also Fig. S5.

Figure 5. PFKFB3 accelerates glycolysis in HSCs under OXPHOS inhibition in an AMPK-dependent manner

(A) Experimental design of real-time ATP analysis using GO-ATeam2 knock-in BMMNCs. Ba-M was used in experiments with oligomycin. For other experiments, PLFA medium was used. **(B-C)** Evaluation of factors affecting ATP concentration in HSCs (B) and GMPs (C) based on the GO-ATeam2 system. GO-ATeam2 knock-in BMMNCs were incubated with glucose, oligomycin, 2-DG, or glucose plus oligomycin, and the FRET/EGFP ratio was calculated. **(D)** ATP concentration in indicated stem/progenitor fractions in PLFA medium (red bars) alone or PLFA medium plus 2-DG (blue bars). ATP concentration for the last 2 min of the analysis time is shown. Data is summarized

bioRxiv preprint doi: https://doi.org/10.1101/2023.03.16.532898; this version posted March 18, 2023. The copyright holder for this preprint (which was not certified by peer review) is the author/funder, who has granted bioRxiv a license to display the preprint in perpetuity. It is made available under aCC-BY-NC-ND 4.0 International license.

from Figure 5B-C and Supplemental Figure 5A-D. Each group represents at least 110 cells. Data are representative results of pooled samples from three biological replicates. **(E)** ATP concentration in indicated stem/progenitor fractions in Ba-M plus glucose (dark blue bars) or Ba-M plus glucose and oligomycin (orange bars). ATP concentration for the last 1 min of the analysis period is shown. Data is summarized from Figure 5B-C and Supplemental Figure 5A-D. Each group represents at least 43 cells. Data are representative results of pooled samples from three biological replicates. **(F-I)** Effects of PFKFB3 or AMPK inhibitors (PFKFB3i or AMPKi, respectively) on ATP concentration in HSCs from GO-ATeam2 mice in Ba-M plus glucose only (F) or Ba-M plus glucose and oligomycin (G). ATP concentrations for the last 1 min of the analysis period are shown in (H) and (I) for glucose only and glucose with oligomycin groups, respectively. Each group represents at least 90 cells. Data are representative results of pooled samples from three biological replicates. **(J)** Experimental schema for cell cycle assay and real-time ATP concentration analysis after overexpression of *Pfkfb3*. **(K)** Cell cycle status of *Pfkfb3*-overexpressing (*Pfkfb3*OE) and *mock*-transduced HSCs. **(L-O)** Effects of inhibitors on ATP concentration in *Pfkfb3*-overexpressing GO-ATeam2^{+} HSCs. Cells were exposed to vehicle (Ctl) (L), 2-DG (M), oligomycin (N), or glucose 12.5 mg/dL and oligomycin (O), and ATP concentrations for the last 1 (L, N, and O) or 2 min (M) of the analysis period were calculated. Data are representative results of pooled samples from three biological replicates.

Data are presented as mean ± SD. * $p \leq 0.05$, ** $p \leq 0.01$, *** $p \leq 0.001$ as determined by Student's *t*-test (D, E, and K-O) or one-way ANOVA followed by Tukey's test (H and I). See also Fig. S5.

Figure 6. PFKFB3 methylation by PRMT1 enables ATP production by cell-cycling HSCs.

(A) Normalized *Pfkfb3* mRNA counts based on RNA sequencing of PBS-treated (red) or 5-FU-treated (blue) HSCs. Data are representative results of pooled samples from three biological replicates. **(B)** Quantification of mean fluorescent intensity (MFI) of PFKFB3 protein in PBS- or 5-FU-treated HSCs. The lower part of the graph shows representative images of immunocytochemistry of PFKFB3 in each group. n = 26–27 single HSCs for each group. The data are representative results from two independent experiments. **(C)** Quantification of MFI of phosphorylated-PFKFB3 (p-PFKFB3) protein in PBS- or 5-FU-treated HSCs. The lower part of the graph shows representative images of immunocytochemistry of p-PFKFB3 in each group. n = 27 single HSCs for each group. The data are representative results from two independent experiments. **(D)** Quantification of mean fluorescence intensity (MFI) of p-PFKFB3 in HSCs treated with glucose (200mg/dL); glucose plus oligomycin (1 μM); and glucose, oligomycin, and dorsomorphin (100 μM)

bioRxiv preprint doi: https://doi.org/10.1101/2023.03.16.532898; this version posted March 18, 2023. The copyright holder for this preprint (which was not certified by peer review) is the author/funder, who has granted bioRxiv a license to display the preprint in perpetuity. It is made available under aCC-BY-NC-ND 4.0 International license.

for 5 min. The lower part of the graph shows representative images of immunocytochemistry of p-PFKFB3 in each group. n = 32–36 for each group. The data are representative results from two independent experiments. **(E)** Normalized *Prmt1* mRNA counts based on RNA sequencing of PBS-treated (red) or 5-FU-treated (blue) HSCs. Data are representative results of pooled samples from three biological replicates. **(F)** MFI quantification of methylated-PFKFB3 (m-PFKFB3) in PBS- or 5-FU-treated HSCs. The lower part of the graph shows representative images of immunocytochemistry of m-PFKFB3 in each group. n = 23–41 for each group. The data are representative results from three independent experiments. **(G)** Quantification of MFI of m-PFKFB3 in PBS- or 5-FU-treated HSCs or 5-FU-treated HSCs after 15 min treatment with a PRMT1 inhibitor (90 μg/mL GSK3368715); n = 25–35 single HSCs for each group. The lower part of the graph shows representative images showing immunocytochemistry of m-PFKFB3. Data represent a single experiment. **(H)** Quantitation of m-PFKFB3 in NBDG-positive or -negative HSCs in mice treated with PBS or 5-FU. The lower part of the graph shows representative images of immunocytochemistry of m-PFKFB3 in each group. n = 28–41 for each group. The data are representative results from two independent experiments. **(I-J)** Corrected ATP levels in PBS- (red) or 5-FU-treated (blue) HSCs 15 min after treatment with vehicle (I) or a PRMT1 inhibitor (90 μg/mL GSK3368715) (J). Each group represents at least 101 cells. Data are representative results of pooled samples of two biological replicates. (see "**Time-course analysis of FRET values**" in "**Supplementary Methods**" for details of the correction method used to calculate ATP concentration.) Data are presented as mean ± SD. * $p \leq 0.05$, ** $p \leq 0.01$, *** $p \leq 0.001$ as determined by Student's *t*-test (A-C, E-F, and I-J) or one-way ANOVA followed by Tukey's test (D, G, and H).

Figure 7. PFKFB3 maintains HSC function under proliferative stress.

(A-C) Transplant analysis of *Pfkfb3*-KO or *Pfkfb3*CA-overexpressing HSCs. Experimental design (A). PB chimerism of donor-derived cells at 4 months post-transplant. *Pfkfb3*-KO group, n = 6; *Rosa*-KO group, n = 4; (B) *Pfkfb3* group, n = 5; pMY-IRES-GFP group, n = 4. (C) The data are representative results from two independent experiments. **(D-E)** 5-FU administration after bone marrow reconstruction with *Pfkfb3*- or *Rosa*-KO HSPCs. Experimental schema (D). Behavior of the *Pfkfb3*- or *Rosa*-KO cells in PB after 5-FU administration (E). n = 5 for each group. **(F-K)** Cell cycle analysis and apoptosis assay of *Pfkfb3*- or *Rosa*-KO HSPCs on day 2 post-BMT. Experimental schema (F). Representative plots of Ki67/Hoechst33432 staining of *Rosa*-KO (G) or *Pfkfb3*-KO (H)

bioRxiv preprint doi: https://doi.org/10.1101/2023.03.16.532898; this version posted March 18, 2023. The copyright holder for this preprint (which was not certified by peer review) is the author/funder, who has granted bioRxiv a license to display the preprint in perpetuity. It is made available under aCC-BY-NC-ND 4.0 International license.

HSPCs and summary of analysis (I); summary of *in vivo* BrdU labeling assay (J). Apoptosis assay results (K). n = 4–5 biological replicates for each group. **(L-N)** Cell cycle analysis of *Pfkfb3*CA or *Mock*-overexpressing HSPCs on day 2 after BMT. Experimental Schema (L). Representative plot of Ki67/Hoechst33432 staining for both groups (M) and summary of analysis (N). n = 5 biological replicates for each group. **(O)** Models showing ATP production and regulation in quiescent, OXPHOS-inhibited, and cell-cycling HSCs. Note that the GO-ATeam2 system identified plastic acceleration of glycolysis by PFKFB3 in response to different types of stress maintains ATP levels.

Data are presented as mean ± SD. * $p \leq 0.05$, ** $p \leq 0.01$, *** $p \leq 0.001$ as determined by Student's *t*-test (B, C, E, H, J, K, and N).

Figure 1

bioRxiv preprint doi: https://doi.org/10.1101/2023.03.16.532898; this version posted March 18, 2023. The copyright holder for this preprint (which was not certified by peer review) is the author/funder, who has granted bioRxiv a license to display the preprint in perpetuity. It is made available under aCC-BY-NC-ND 4.0 International license.

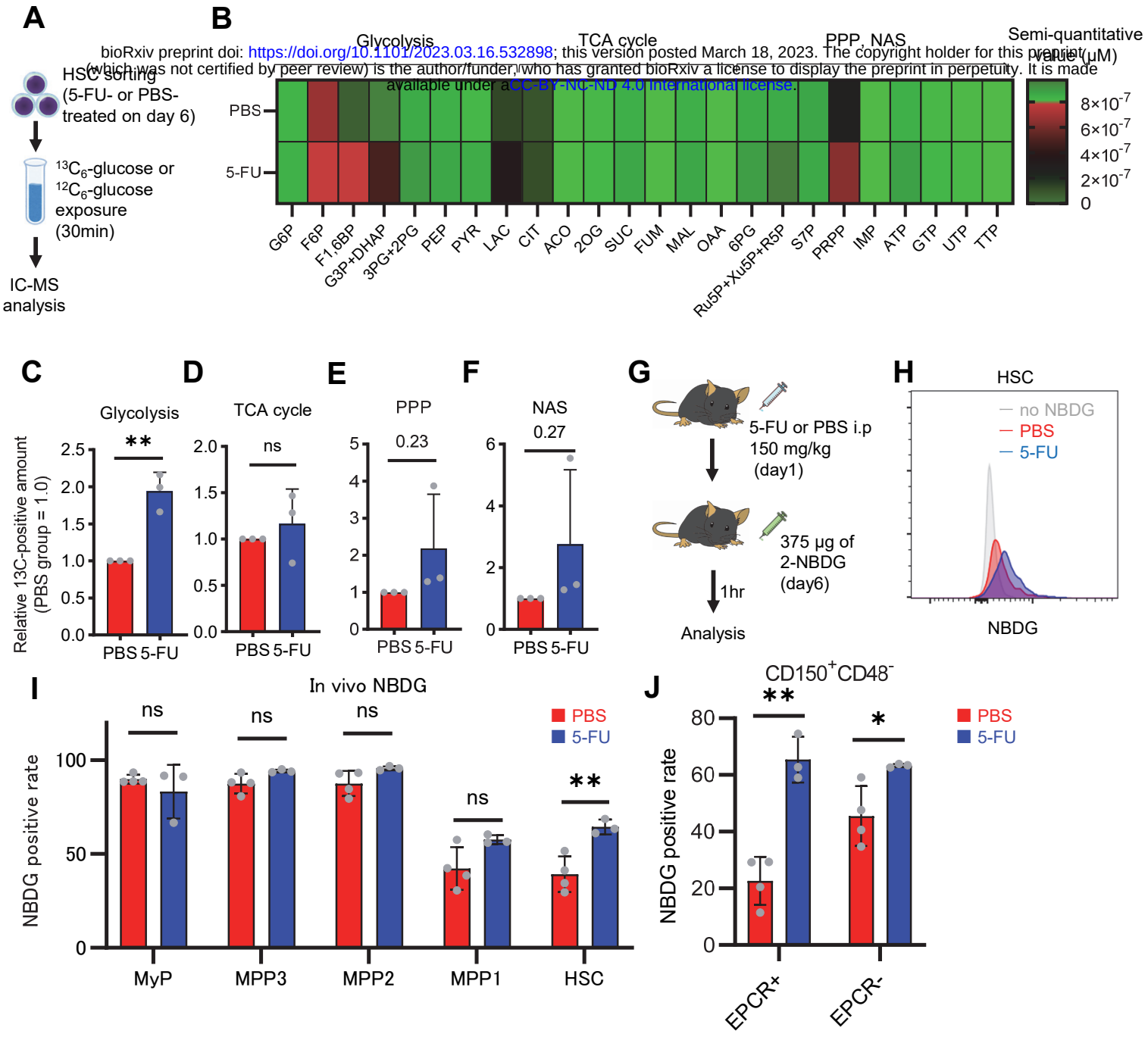

Figure 2

bioRxiv preprint doi: https://doi.org/10.1101/2023.03.16.532898; this version posted March 18, 2023. The copyright holder for this preprint (which was not certified by peer review) is the author/funder, who has granted bioRxiv a license to display the preprint in perpetuity. It is made available under aCC-BY-NC-ND 4.0 International license.

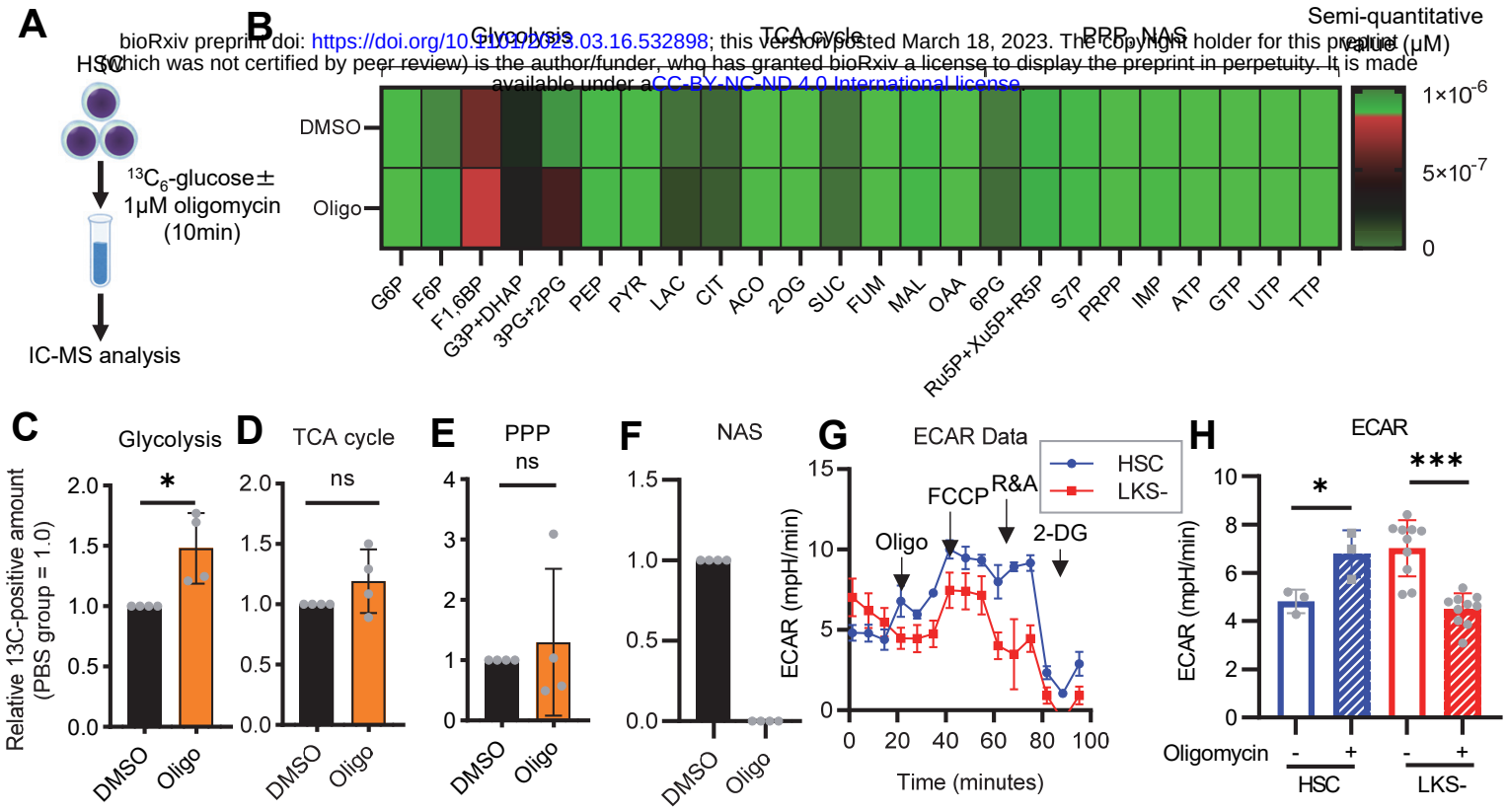

Figure 3

bioRxiv preprint doi: https://doi.org/10.1101/2023.03.16.532898; this version posted March 18, 2023. The copyright holder for this preprint (which was not certified by peer review) is the author/funder, who has granted bioRxiv a license to display the preprint in perpetuity. It is made available under aCC-BY-NC-ND 4.0 International license.

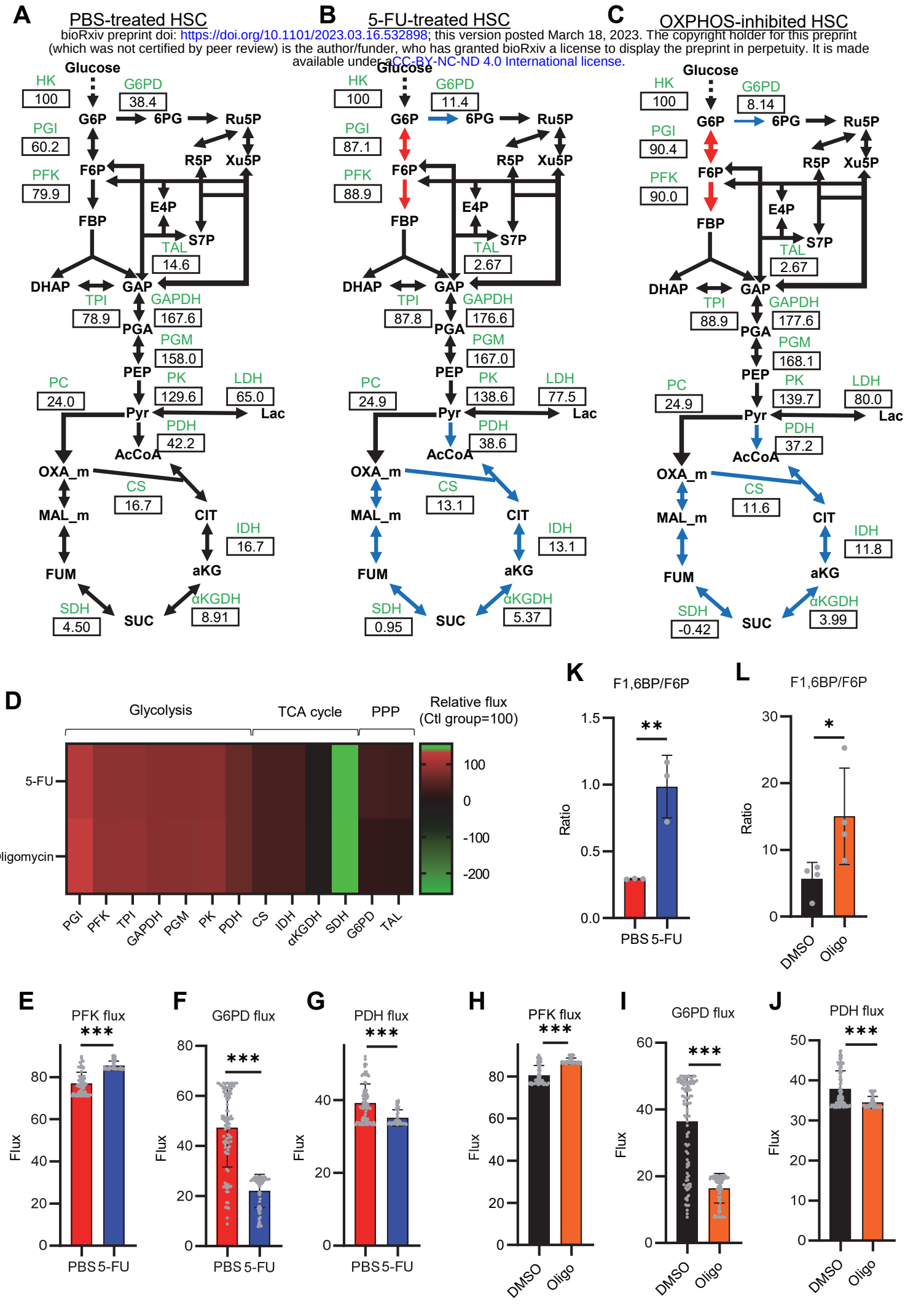

Figure 4

bioRxiv preprint doi: https://doi.org/10.1101/2023.03.16.532898; this version posted March 18, 2023. The copyright holder for this preprint (which was not certified by peer review) is the author/funder, who has granted bioRxiv a license to display the preprint in perpetuity. It is made available under aCC-BY-NC-ND 4.0 International license.

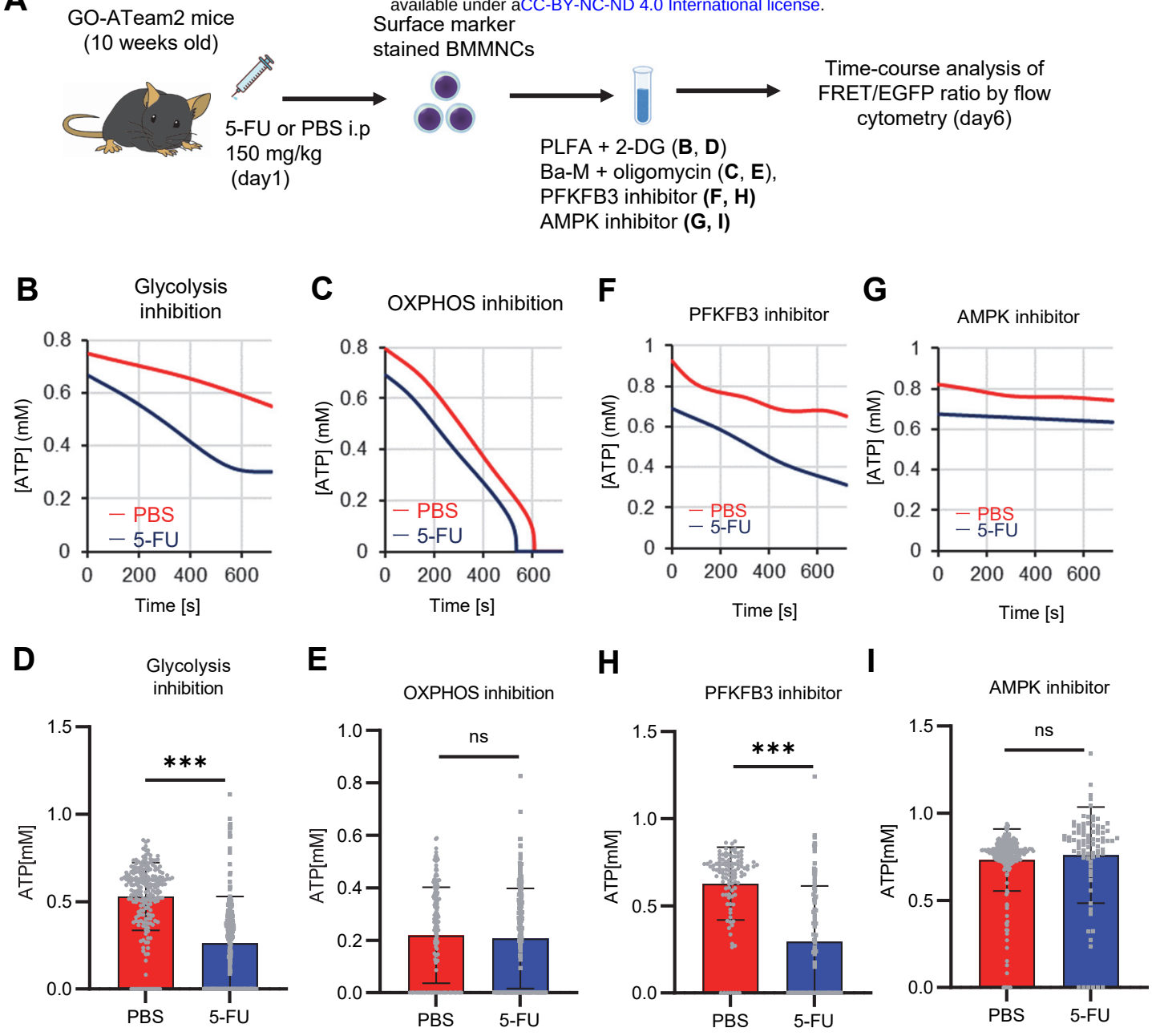

Figure 5

bioRxiv preprint doi: https://doi.org/10.1101/2023.03.16.532898; this version posted March 18, 2023. The copyright holder for this preprint (which was not certified by peer review) is the author/funder, who has granted bioRxiv a license to display the preprint in perpetuity. It is made available under aCC-BY-NC-ND 4.0 International license.

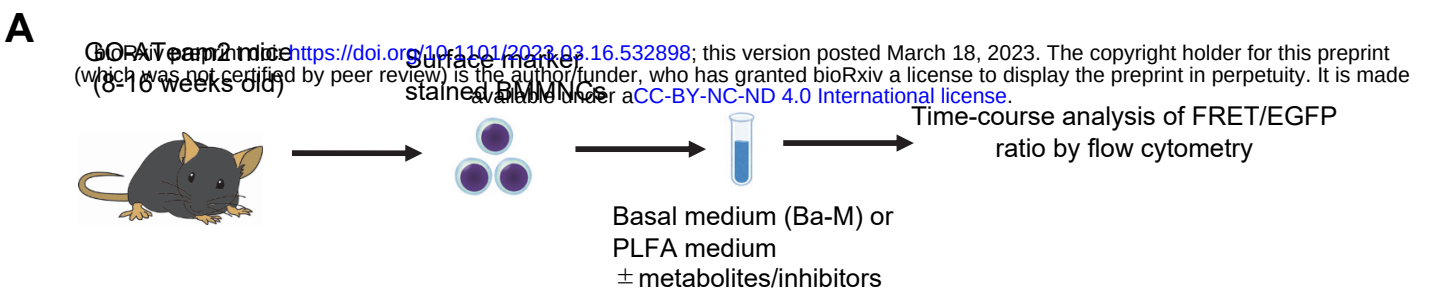

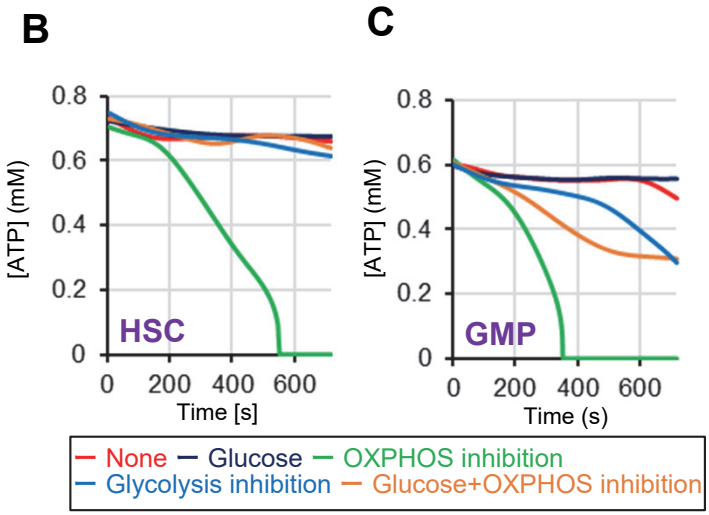

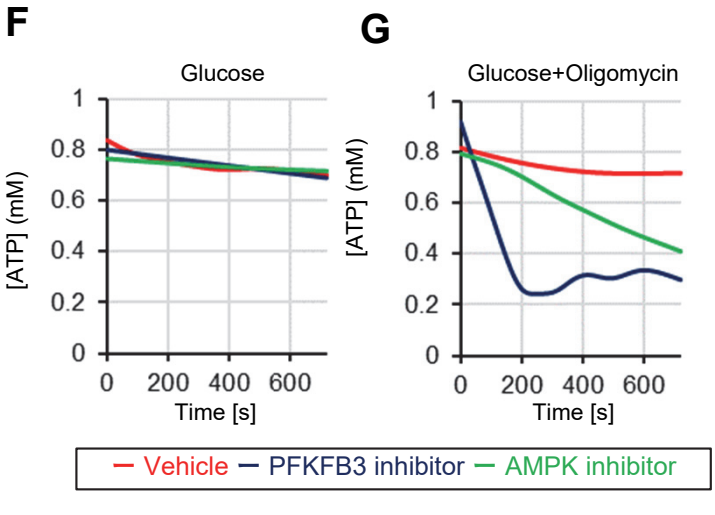

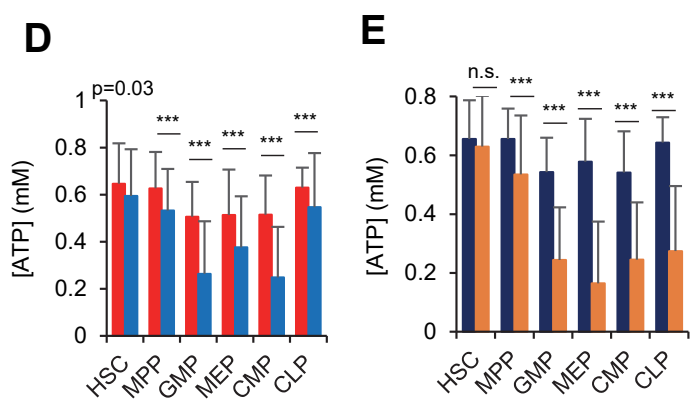

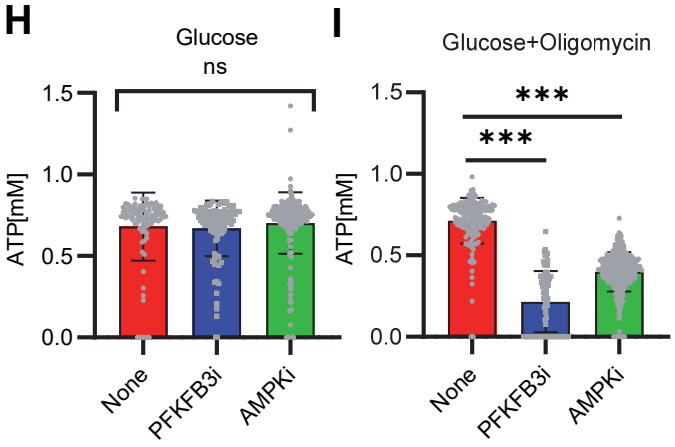

J

Pfkfb3-overexpressed
HSC (WT or GO-ATeam2⁺)

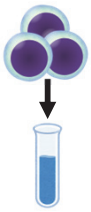

① Cell-cycle assay (WT)
② Time-course analysis of FRET/EGFP ratio by flow cytometry (GO-ATeam2+)

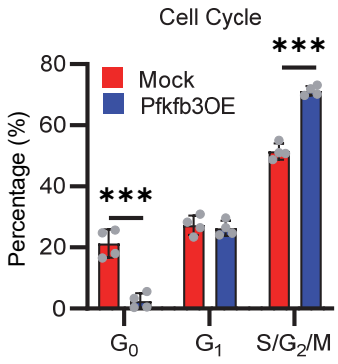

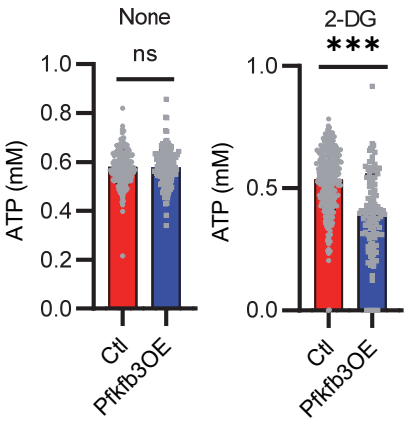

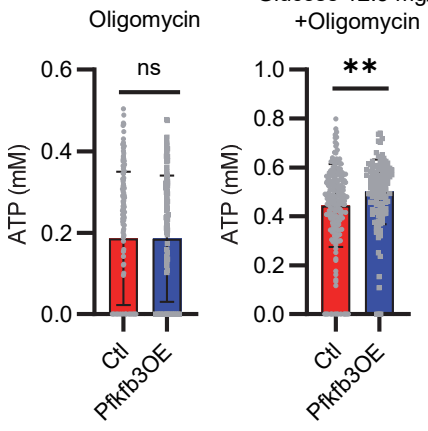

Figure 6

bioRxiv preprint doi: https://doi.org/10.1101/2023.03.16.532898; this version posted March 18, 2023. The copyright holder for this preprint (which was not certified by peer review) is the author/funder, who has granted bioRxiv a license to display the preprint in perpetuity. It is made available under aCC-BY-NC-ND 4.0 International license.

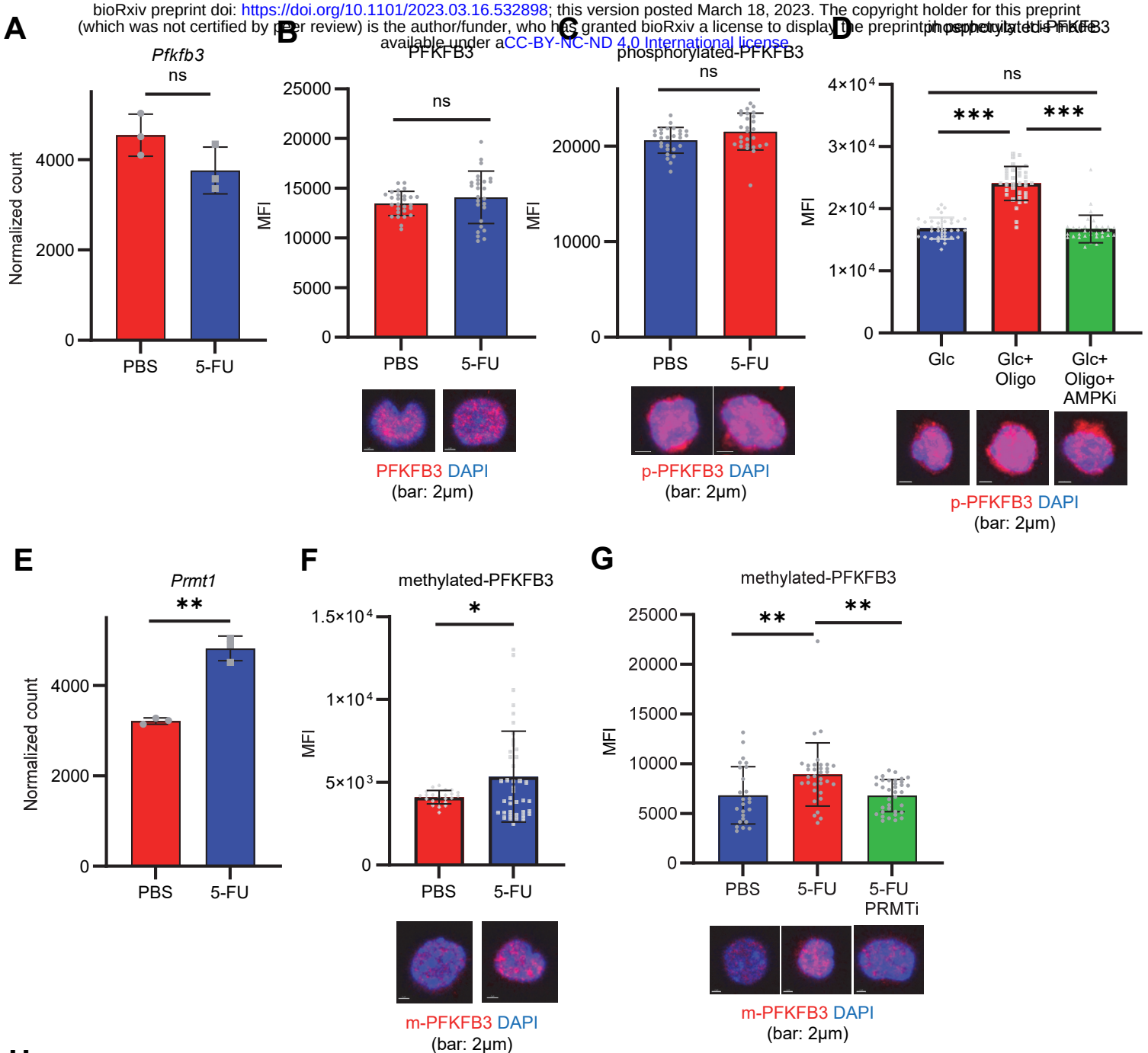

Figure 7

bioRxiv preprint doi: https://doi.org/10.1101/2023.03.16.532898; this version posted March 18, 2023. The copyright holder for this preprint (which was not certified by peer review) is the author/funder, who has granted bioRxiv a license to display the preprint in perpetuity. It is made available under aCC-BY-NC-ND 4.0 International license.